Bioactive Materials 33 (2024) 545–561

Contents lists available at ScienceDirect

Bioactive Materials

journal homepage: www.keaipublishing.com/en/journals/bioactive-materials

Reactive oxygen species (ROS)-mediated M1 macrophage-dependent nanomedicine remodels inflammatory microenvironment for osteoarthritis recession

Chunchun Xue [a,b,c,e,1], Jia Tian [d,1], Zepeng Cui [d,1], Yang Liu [a,b,c], Dawei Sun [a,b,c], Mengting Xiong [a,b,c], Nanxing Yi [a,b,c], Kaiqiang Wang [e], Xiaofeng Li [e], Yongjun Wang [a,b,c,****], Hao Xu [a,b,c,***], Weian Zhang [d,**], Qianqian Liang [a,b,c,*]

[a] Longhua Hospital, Shanghai University of Traditional Chinese Medicine, Shanghai, 200032, China
[b] Spine Institute, Shanghai University of Traditional Chinese Medicine, Shanghai, 200032, China
[c] Key Laboratory of Theory and Therapy of Muscles and Bones, Ministry of Education, Shanghai University of Traditional Chinese Medicine, Shanghai, 201203, China
[d] Shanghai Key Laboratory of Functional Materials Chemistry, School of Chemistry and Molecular Engineering, East China University of Science and Technology, Shanghai, 200237, China
[e] Shanghai Municipal Hospital of Traditional Chinese Medicine, Shanghai University of Traditional Chinese Medicine, Shanghai, 200071, China

ARTICLE INFO

Keywords:
Reactive oxygen species
Osteoarthritis
Inflammatory microenvironment
Macrophages polarization
Apoptosis

ABSTRACT

Osteoarthritis (OA) is a common chronic inflammatory disorder. Effective remodeling of inflammatory microenvironment in the joint is a promising strategy to prevent OA. However, current drugs remain unsatisfactory due to a lack of targeted and effective ways for relieving inflammatory conditions in OA joints. Bortezomib (BTZ), a proteasome inhibitor, could effectively inhibit proinflammatory cytokines but with poor accumulation in the inflammatory tissues. To overcome the shortcomings of BTZ delivery and to improve the efficacy of OA therapy, herein, we designed a novel nanomedicine (denoted as BTZ@PTK) by the co-assembly of BTZ and an amphiphilic copolymer (denoted as PTK) with ROS-cleaved thioketal (TK) linkages. The TK units in BTZ@PTK are first cleaved by the excessive ROS at OA sites, and then triggered the controlled release of BTZ, resulting in the accurate delivery and the inflammatory microenvironment remodeling. Accordingly, BTZ@PTK suppressed ROS generation and proinflammatory cytokines while promoting M1 macrophage apoptosis in lipopolysaccharide (LPS)-activated RAW264.7 macrophages or LPS/IFN-γ-treated primary macrophages, which leads to a better effect than BTZ. In OA mice, BTZ@PTK passively accumulates into inflamed joints to attenuate pain sensitivity and gait abnormality. Importantly, BTZ@PTK treatment successfully ameliorates synovitis with the reduction of synovial hyperplasia and synovitis scores by suppressing M1 macrophage polarization and promoting M1 macrophage apoptosis in the synovium, thereby delaying cartilage damage. Collectively, BTZ@PTK can effectively modulate inflammatory microenvironment for OA recession by activating M1 macrophage apoptosis and inhibiting M1macrophage-mediated inflammatory response.

Peer review under responsibility of KeAi Communications Co., Ltd.

* Corresponding authors. Longhua Hospital, Shanghai University of Traditional Chinese Medicine, Shanghai, 200032, China.
** Corresponding author. Shanghai Key Laboratory of Functional Materials Chemistry, School of Chemistry and Molecular Engineering, East China University of Science and Technology, Shanghai, 200237, China.
*** Corresponding author. Longhua Hospital, Shanghai University of Traditional Chinese Medicine, Shanghai, 200032, China.
**** Corresponding author. Longhua Hospital, Shanghai University of Traditional Chinese Medicine, Shanghai, 200032, China.
E-mail addresses: wangyongjun@shutcm.edu.cn (Y. Wang), xuhao@shutcm.edu.cn (H. Xu), wazhang@ecust.edu.cn (W. Zhang), liangqianqian@shutcm.edu.cn (Q. Liang).
[1] These authors contributed equally to this work.

https://doi.org/10.1016/j.bioactmat.2023.10.032
Received 6 May 2023; Received in revised form 9 October 2023; Accepted 30 October 2023

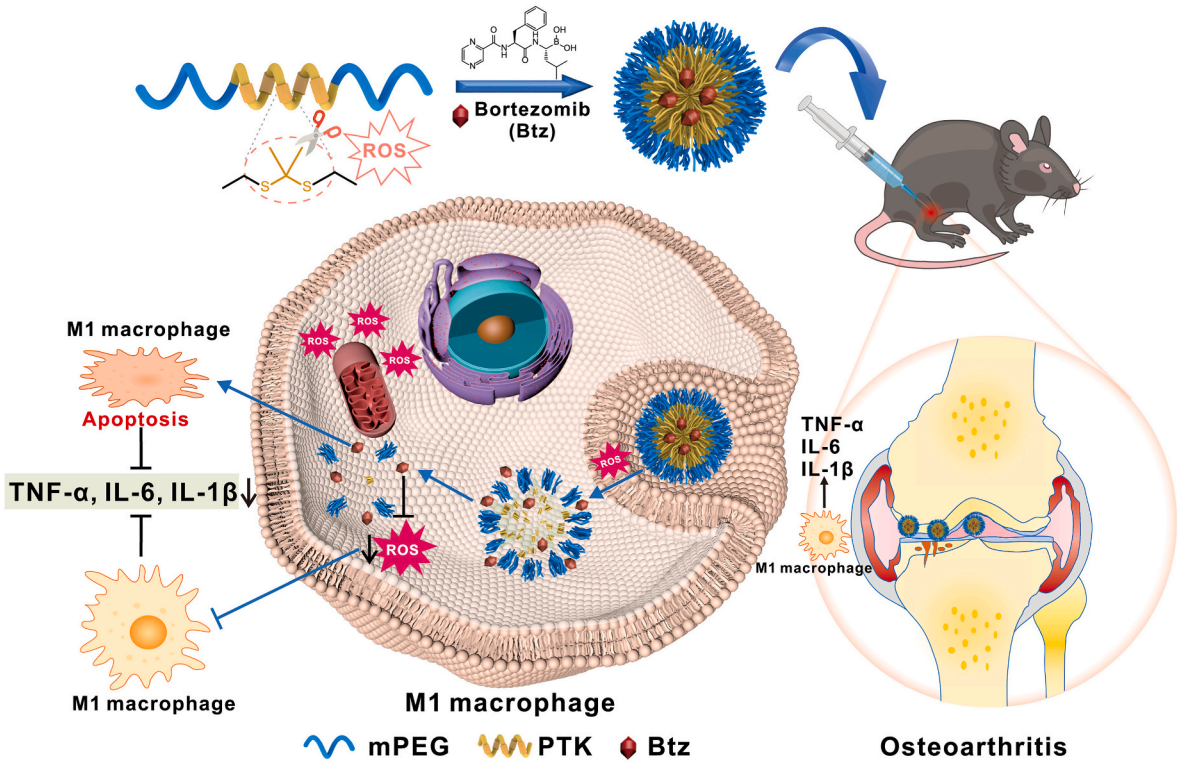

Scheme 1. ROS-modulated nanomedicine for M1 macrophage-dependent inflammatory microenvironment modification and its working mechanism on OA treatment.

1. Introduction

Osteoarthritis (OA) is a widespread and degenerative joint disease affecting more than 240 million people globally [1–3]. Patients with OA often suffer chronic pain and joint dysfunction, which seriously reduces productivity and quality of life [4]. In clinics, pharmacologic treatments such as non-steroidal anti-inflammatory drugs (NSAIDs) are typically managed to relieve symptoms of OA [5], however, medications cannot prevent the OA progression. Therefore, there still exists an urgent need to seek novel anti-inflammatory drugs to slow the OA progression.

Microenvironment in the joint is critical for maintaining joint homeostasis. During OA microenvironment, chronic synovitis and cartilage degeneration are primarily two pathological characteristics. Increasing evidence has been revealed that synovial inflammation precedes cartilage degeneration [6,7]. Importantly, macrophages in synovial tissue are considered to be the most important cells that initiate and perpetuate inflammation. Among the inflammatory tissues, more macrophages are activated as proinflammatory M1 macrophages, producing a series of inflammation cytokines to sustain and aggravate joint inflammation [8]. On the contrary, M2 macrophages with the capabilities of anti-inflammatory, mainly assist in tissue repair and inflammation resolution [9]. Thus, directly inhibiting M1 or promoting M1 to M2 re-polarization are considered to be effective therapeutic strategies.

It has been shown that most of OA patients suffer from synovitis often characterized by increased abundance and activation of M1 macrophages in synovium that produce reactive oxygen species (ROS) [10]. The rich ROS is a typical characteristic of OA inflamed microenvironment. Increased ROS production contributes to joint inflammation, deregulation of matrix synthesis and degradation and cartilage damage [11–13]. OA models also have found that reducing ROS could alleviate OA synovitis and cartilage damage [14]. Thus, the elimination of excess ROS has proven to be of great help in OA microenvironment and recovery [15]. Several studies have employed ROS scavenging nanozymes for combating inflammatory arthritis [16,17]. Based on the above, we are considering if we can develop a nanomedicine that not only consumes ROS but also works synergistically with drugs that suppress macrophage proinflammatory polarization in the inflammatory milieu.

Our previous study found that Bortezomib (BTZ), a proteasome inhibitor, effectively inhibited the M1 macrophage in synovial cells, preventing cartilage degradation during OA progression [18]. Also, BTZ could repress proinflammatory cytokines in collagen-induced arthritis mice [19] and the overexpression of MMP-13 in tumor necrosis factor-α (TNF-α) treated human chondrocytes [20], suggesting that for OA treatment, BTZ plays an effective role against synovitis and cartilage damage by inhibiting M1 macrophage inflammatory response. However, BTZ has short half-lives and it is rapid to eliminated by oxidative de-boronation via CYP450 enzymes during metabolism [21], resulting in poor accumulation in the inflamed tissues. Therefore, there is a pressing requirement to create a persistent drug delivery strategy that exhibits sustained anti-inflammation in inflammatory tissues.

Herein, we presented a novel and versatile strategy for the construction of a degradable nanomedicine and its application in osteoarthritis recession by inflammatory microenvironment remodeling (Scheme 1). The nanomedicine (denoted as BTZ@PTK) was prepared by the co-assembly of BTZ and an amphiphilic copolymer with ROS-cleaved thioketal (TK) linkages. During the primary ROS responsiveness, the TK units in nanomedicine could be effectively cleaved by the overexpressed ROS at OA joints, which not only consumed the ROS in the lesion sites, but also triggered the controlled release of BTZ specifically in inflammatory tissue to exert anti-inflammation effect. The release behavior and deformation of BTZ@PTK were monitored by UV–vis spectrometry and dynamic light scattering (DLS) analysis, respectively. Moreover, the efficient ROS sensitive anti-inflammatory function against OA by utilizing this nanomedicine was assessed by both *in vitro* and *in vivo* approaches. Furthermore, the underlying biological mechanism associated with macrophage-dependent remodeling of the inflammatory microenvironment for OA regression was explored.

2. Material and methods

2.1. Materials

3-Mercaptopropionic acid, 1-cyanato-6-isocyanatohexane, BTZ, and monomethoxy poly(ethylene glycol (mPEG) were purchased from Sigma-Aldrich. NaOH and $LiAlH_4$ were bought from Macklin (Shanghai, China). The solvents used in the experiments included tetrahydrofuran, and DMSO was purchased from Aladdin (Shanghai, China). Anhydrous THF and dichloromethane (DCM) were dried by distilling before use.

2.2. Synthesis of ROS-responsive polymer PTK

Hydroxyl-terminal TK linker (TK-OH) (0.20 g, 0.90 mmol) was dissolved in 10 mL of anhydrous DCM under strong magnetic stirring. 1-Cyanato-6-isocyanatohexane (168 mg,1 mmol) dissolved in 8 mL of super dry DCM solution was slowly added into the flask under nitrogen atmosphere. After stirring at 0 °C for 1 h, the above mixture was refluxed at 40 °C overnight under stirring. Next, mPEG dissolved in 5 mL of anhydrous DCM solution was injected and the mixture was stirred for another 24 h. Finally, the crude product was concentrated and then precipitated in cold diethyl ether for several times. PTK was obtained as a white solid powder after filtration and drying in vacuum (yield: 65%).

2.3. Preparation and characterizations of the BTZ@PTK nanoparticles

The BTZ@PTK nanoparticles (NPs) were prepared via the classic nanoprecipitation method. Simply, BTZ (2.0 mg) and PTK polymer (20.0 mg) were fully dissolved in DMSO (1.0 mL). After mixing evenly for 2 h, the mixture was slowly added into 3 mL of deionized water. Then the suspension was dialyzed against deionized water to remove DMSO and the unencapsulated BTZ (MWCO = 3500) for 48 h. IR780@PTK NPs were prepared by using a similar method to perform *in vivo* fluorescence bioimaging.

To determine the loading content of BTZ in BTZ@PTK, the BTZ@PTK nanoparticles were lyophilized and then re-dissolved in DMSO. The concentration was calculated by UV–vis absorption of BTZ@PTK at the wavelength of 268 nm according to the BTZ standard curve. The drug loading content (DLC) of BTZ@PTK NPs was obtained according to the following formula:

DLC (%) = (weight of drug in NPs)/(weight of drug-loaded NPs)* 100% …… (1)

2.4. In vitro BTZ release

The BTZ@PTK NPs were obtained according to the above method and then re-dispersed in PBS solution. Subsequently, the BTZ@PTK suspension was transferred to a dialysis tube (MWCO 1.0 kDa) and further buried in PBS (pH = 7.4) or PBS (pH = 7.4) with 1.0 mM H_2O_2 solution at 37 °C. At a predetermined interval, 2.0 mL external buffer was taken out and the same volume of fresh buffer was added. After placing at room temperature for 24 h, the absorbance of released BTZ was measured by UV–vis spectrophotometer. The cumulative BTZ release was calculated as follows:

Cumulative release (%) = $(M_t / M) \times 100\ \%$ ……(2)

Where M_t was the amount of BTZ released at time t and M was the total amount of BTZ.

2.5. ROS-responsiveness of BTZ@PTK in human OA synovial fluid

Three samples of Human OA synovial fluid were collected in Longhua Hospital. The patients' consent, as well as approval of the ethics committees of Longhua Hospital, were obtained before harvesting human tissue samples (No. 2021LCSY055). 9,10-Diphenyl anthracene (An) was used as the probe of ROS responsiveness. An@PTK nanomedicine (5.5 mg/mL) was prior prepared via a similar strategy with BTZ@PTK in the main text. The An@PTK solution (20 μL) was added into 2.0 mL of PBS and human OA synovial fluid, respectively. The fluorescence spectra of An@PTK in both PBS and human OA synovial fluid were tested (λ_{ex} = 350 nm).

2.6. Mice and osteoarthritic model

C57BL/6 male mice were purchased and housed at Shanghai Research Center of Model Organisms. And all experimental procedures were approved by the Institutional Animal Care and Use Committee (No. 2018-0026). Ten-week-old C57BL/6 male mice weighing 23–27 g were subjected to surgically induce OA by destabilization of the medial meniscus (DMM) as previously described [22]. Briefly, the mice were anesthetized by isoflurane, the medial capsule of the right knee was incised, and then, the medial meniscus was sectioned with microsurgical scissors from its anterior attachment to the tibia. All mice were allowed to move freely in the cages after surgery.

After the OA model was induced, forty mice were randomly assigned into five groups (n = 8 per group): Control (Con), DMM model followed by treatment with PBS, PTK, BTZ and BTZ@PTK (10 μL), normal mice as a control. The dose of free BTZ was equivalent to that loaded in BTZ@PTK (0.05 mg/kg, in 10 μL PBS/intra-articular (i.a.) injection). Each treatment groups begin to treat at 4 weeks post-OA surgery with a weekly intra-articular injection for 8 weeks. During the process, the efficacy was evaluated on the day of surgery prior to DMM and at weeks 4, 8, and 12 after the surgery and at 12 weeks post-DMM operation all mice were euthanized and tissues were collected for further analyses.

2.7. Ultrasound acquisition and analysis

The joint space volume was detected by ultrasound imaging on a high-resolution small-animal US system (Vevo 3100, FUJIFILM VisualSonics Inc.) as described previously [23]. During general anesthesia, mice were maintained with 2%–3% isoflurane inhalation throughout the entire procedure. The right knee was flexed at approximately 130° angle and applied coupling gel, then we used a US head to observe a triangular region of interest (ROI) with a bright US signal in a B-mode image. The ROI consists of synovium, meniscus, soft tissues, and synovial fluid space, which was reconstructed as a 3D image from 20 to 30 B-mode measurements to obtain the ROI volume using software, which we refer to as "joint space volume".

2.8. Paw thermal withdrawal latency (PTWL)

The PTWL testing is in response to nociceptive responses of thermal stimuli, which was determined by the radiant thermal apparatus (UGO BASILE, Italy, 37370). The mice were placed in a plastic chamber (10cm × 10cm × 12 cm) to adapt to the environment for 1–2h before testing. When the mice stopped exploring and stood quietly, the radiant heat source was positioned under the glass floor directly beneath the mid-plantar surface of the right hind paw, the intensity of the light source was set to 20 and the cut off time of 20 s. We recorded the latency time, repeated the assessment 3 times, each at an interval of 5–10 min, and calculated the mean.

2.9. Gait

The gait parameters were recorded and analyzed using a DigiGait imaging system (Columbus Instruments, USA, XL Gait Controller) as previously described [24]. Briefly, mice were placed individually in the walkway and allowed to walk freely and traverse from one side to the other of the walkway at a specific speed (10 cm/s), while a video camera

captured ventral images. The following indexes of the right hind limb were observed including stride length, stride, brake and stance.

2.10. Histology and immunohistochemistry (IHC) staining

For all the histological staining, the samples were fixed in 10% NBF solution, decalcified in 14% (ethylenediamine tetraacetic acid) EDTA solution (pH = 7.4), dehydrated and embedded in paraffin. Serial midsagittal sections (4 μm thick) were cut and stained with Alcian Blue/hematoxylin/Orange G (ABOG) or Safranin O/Fast green (SO/FG) to assess OA-related morphometric changes. Synovitis score [25] and OARSI score [26]applied to the medial tibial plateau were graded as described previously and cartilage areas were analyzed by two independent observers.

For IHC staining, paraffin sections (4 μm thick) were rehydrated and digested in Proteinase K solution (10 mg/mL) for 15 min at 37 °C. Sections were treated with first antibodies (Col 2a1, ab34712, 1:200; Col X, ab58632, 1:5000; MMP13, ab39012, 1:800; Nitege, MD Biosciences, 1042003, 1:200) diluted in antibody dilution solution of a Polink-2 plus polymer HRP detection system kit (ZSGB-BIO, PV-9001/PV9002) overnight at 4 °C, coloration with 3, 3′-Diaminobenzidine (DAB) solution, counterstained with hematoxylin and mounted. The stained sections were scanned with an Olympus VS120 whole slide imager or a light microscope (Leica, DM6).

2.11. Immunofluorescence (IF) staining

After deparaffinization, rehydration and antigen retrieval, the sections of knee joints were incubated with primary antibodies (F4/80, ab204266, 1:400; iNOS, ab209027, 1:200) at 4 °C overnight, and then incubated with fluorescent-labeled secondary antibodies for 30 min. After being counterstained with DAPI, the sections were imaged using a fluorescent (Olympus, VS120).

2.12. TUNEL staining

TUNEL staining was performed using the DeadEnd™ Fluorometric TUNEL SystemKit (Promaga, #G3250). After mounting with DAPI reagent to stain nuclei, the samples were observed with a fluorescence microscope (Olympus, VS120).

2.13. RAW 264.7 cell line

RAW 264.7 cells were purchased from Shanghai Jinyuan Biotechnology Co. Ltd. and cultured in Dulbecco's modified Eagle's medium (DMEM) supplemented with 10% FBS, 1% penicillin/streptomycin at 37 °C in a humidified 5% CO_2 atmosphere. The cells were stimulated with or without 1 μg mL^{-1} LPS for 6 h, followed by treatment with PBS, PTK, BTZ, and BTZ@PTK (1 nM) for another 24 h, and cells cultured in the fresh medium were used as a control. Then the culture supernatant was collected for ELISA analysis and the collected cells were for ROS detection, apoptosis analysis or qPCR assay.

2.14. Macrophages culture

Bone marrow derived macrophages (BMDMs) were cultured as previously reported [27]. Briefly, BMDMs were collected from 8 to 10-week-old male C57BL/6 mice and add red blood cell lysis buffer to remove red blood cells. Then cells were resuspended and cultured in DMEM supplemented with 10% FBS, 1% penicillin/streptomycin and 20 ng/ml of macrophage colony stimulating factor (M-CSF, Novoprotein, CB34) at 37 °C and 5% CO_2. On day 5, cells were treated with or without 1 μg/mL of LPS plus 100 ng/mL of IFN-γ for 6 h followed by treatment with PBS, PTK, BTZ, BTZ@PTK (1 nM) for another 24 h, cells cultured in fresh medium were used as the control. The cells were collected for ROS detection, apoptosis analysis or qPCR assay. The concentrations of inflammatory factors in the supernatants of cells were determined by ELISA. All experiments were performed three times for each new experiment.

2.15. ROS detection

The level of intracellular ROS was monitored using the 2,7-dichlorofluorescein diacetate (DCFH-DA) assay kit (Yeasen, #50101ES01) following the manufacturer's specifications. Cells were incubated by ROS fluorescent probe DCFH-DA (10 μM) for 2 h and then observed by microscope (ECLIPSE Ti2-U, Nikon). Then through the same procedure, the ROS generation was analyzed by flow cytometry using a flow cytometer (Accuri C6 Plus, BD Biosciences).

2.16. Flow cytometric analysis

The apoptotic cell incidence was evaluated by the Annexin V-phycoerythrin (PE)/propidium iodide (PI) apoptosis detection kit (BD Biosciences, #556547) according to the manufacturer's instructions. Briefly, treated M1 macrophages were collected and washed with PBS buffer, then incubated with 5 μL Annexin V-PE and 5 μL PI for 20 min at room temperature in the dark. Finally, ending buffer was added, and cell apoptotic rate was analyzed using a flow cytometer (Accuri C6 Plus, BD Biosciences). The apoptosis incidence was calculated by the percentage of early apoptotic (Annexin V+/PI-) cells plus the percentage of late apoptotic (Annexin V+/PI+) cells.

For the p-STAT3 detection, RAW 264.7 cells were stimulated with LPS (1 μg/mL) in the presence or absence of BTZ (1 nM) treatment for 2 h. Cells were collected and fixed in a single step using BD Phosflow™ Lyse/Fix buffer (#558049) for 10 min at 37 °C. Subsequently, cells were permeabilized in BD Phosflow™ Perm Buffer III (#558050) for 30 min on ice and washed twice in BD Pharmingen™ Stain Buffer (#554656) and stained with Alexa Fluor® 488 mouse anti-Stat3 (pY705) antibody (BD, #557814) for 30 min at room temperature. Samples were analyzed on a BD FACSCalibur™ instrument.

2.17. RNA extraction and real-time PCR (RT-PCR)

Total RNA was extracted using an EZ-press RNA Purification Kit (EZBioscience, #B0004D-100) and was reversely transcribed using the Reverse Transcription Kit (Abm, #G490). cDNA was amplified by RT-PCR using an SYBR Green qPCR Kit (StarLighter, #FS-Q1002) using sequence-specific primers (Table S1). Each sample was repeated with at least 3 independent RT-PCR amplifications. Fold changes of genes of interest were calculated using control samples as 1.

2.18. Enzyme-linked immunosorbent assay (ELISA)

The concentrations of interleukin (IL)-1β and TNF-α in the supernatants of M1 macrophages were determined by using the Mouse IL-1 beta ELISA Kit (absin, #abs520001) and Mouse TNF alpha ELISA Kit (absin, #abs520010) according to the manufacturer's instructions, respectively.

2.19. RNA sequencing

Total RNA was isolated using the Trizol Reagent (Invitrogen Life Technologies), after which the concentration, quality and integrity were determined using a NanoDrop spectrophotometer (Thermo Scientific). Three micrograms of RNA were used as input material for the RNA sample preparations. Sequencing libraries were generated according to the following steps. Firstly, mRNA was purified from total RNA using poly-T oligo-attached magnetic beads. Fragmentation was carried out using divalent cations under elevated temperature in an Illumina proprietary fragmentation buffer. First strand cDNA was synthesized using random oligonucleotides and Super Script II. Second strand cDNA

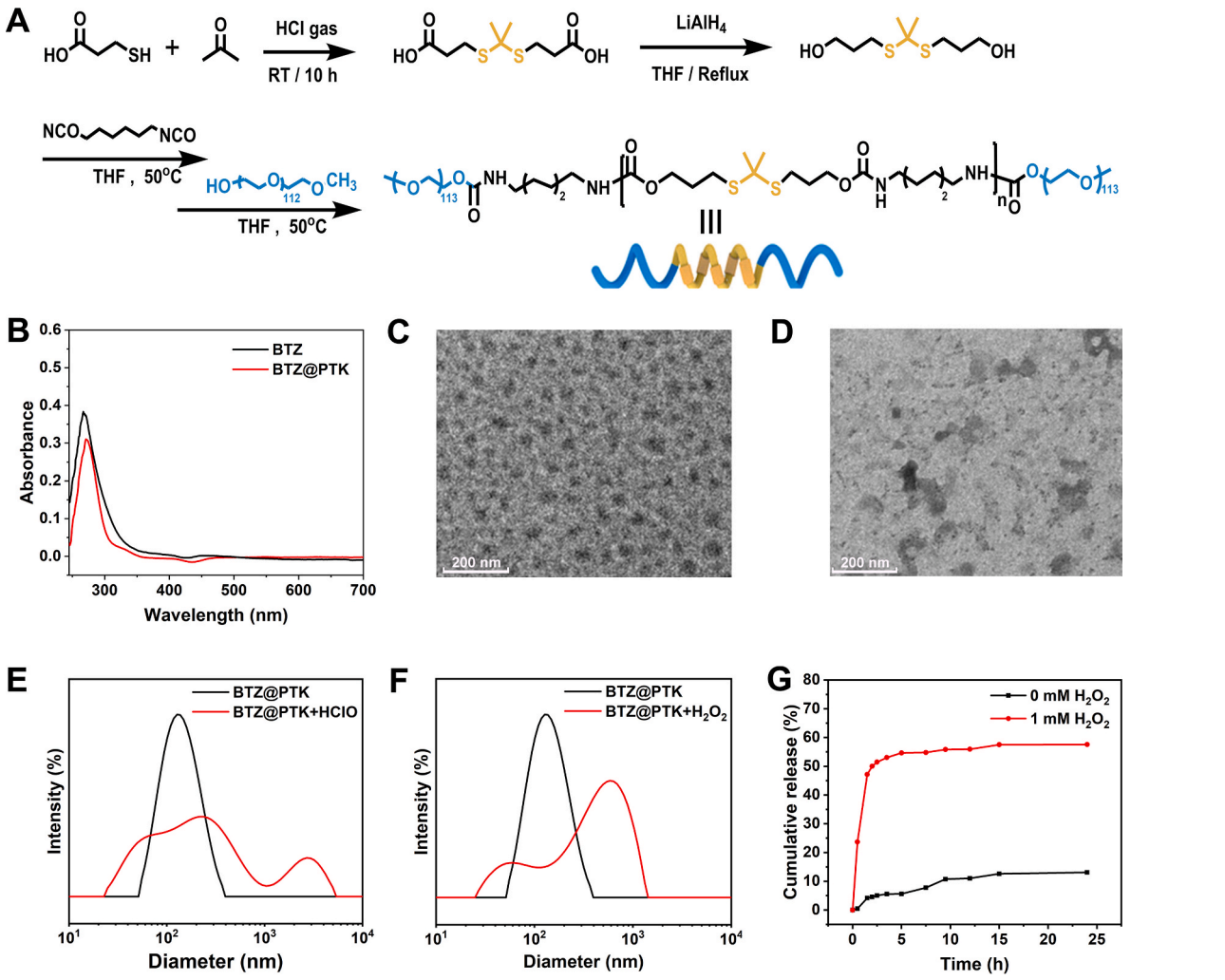

Fig. 1. Characterization of BTZ@PTK.
(A) Schematic illustration of the synthesis of PTK. (B) UV–vis spectra of BTZ and BTZ@PTK. (C) A TEM image of BTZ@PTK in PBS. (D) A TEM image of BTZ@PTK in the buffer solution with extrinsic ROS source. (E) DLS curves of BTZ@PTK with and without HClO solution. (F) DLS curves of BTZ@PTK with and without H_2O_2 solution. (G) Release profiles of BTZ@PTK with and without 1.0 mM H_2O_2 solution.

synthesis was subsequently performed using DNA Polymerase I and RNase H. Remaining overhangs were converted into blunt ends via exonuclease/polymerase activities and the enzymes were removed. After adenylation of the 3′ends of the DNA fragments, Illumina PE adapter oligonucleotides were ligated to prepare for hybridization. To select cDNA fragments of the preferred 400–500 bp in length, the library fragments were purified using the AMPure XP system (Beckman Coulter, Beverly, CA, USA). DNA fragments with ligated adaptor molecules on both ends were selectively enriched using Illumina PCR Primer Cocktail in a 15-cycle PCR reaction. Products were purified (AMPure XP system) and quantified using the Agilent high sensitivity DNA assay on a Bioanalyzer 2100 system (Agilent). The sequencing library was then sequenced on NovaSeq6000 platform (Illumina) Genekinder Medicaltech (Shanghai) Co., Ltd, China.

2.20. Western blot analysis

RAW 264.7 cells were seeded in 6-well plate and stimulated with LPS (1 μg/mL) in the presence or absence of BTZ (1 nM) treatment for 2 h. Proteins were extracted from RAW264.7 cells using RIPA lysis buffer (Beyotime, Shanghai, China). Protein contents were determined by the BCA protein assay kit (Beyotime, Shanghai, China) and then blotted on the nitrocellulose filter membranes (Millipore, USA). Specific antibodies were performed for incubation and the proteins were visualized by ChemiDOC Western blot technique (BIO-RAD). The antibodies used for Western blot were p-JAK1 (Affinity, # AF2012, 1:1000), p-JAK2 (Affinity, # AF3012, 1:1000), and β-actin (CST, 8480S, 1:1000). β-actin was used as an internal control.

2.21. Statistics

Data were presented as mean ± standard deviation (SD) and were analyzed using the GraphPad Prism software (8.0). One-way analysis of variance (*ANOVA*) followed by least significant difference (*LSD*) was used for multiple comparisons by SPSS software (version, 21.0, IBM SPSS, Armonk, NY, USA). A nonparametric paired comparison was applied for the statistical analysis of the OARSI score and synovitis score. P value < 0.05 was considered statistically significant.

3. Results and discussion

3.1. Synthesis and characterization of PTK polymers

Targeting the overexpressed ROS at inflammatory joints, an amphiphilic copolymer (PTK) with thioketal (TK) linkages which could be cleaved by ROS was synthesized and used as nanocarriers. While under a

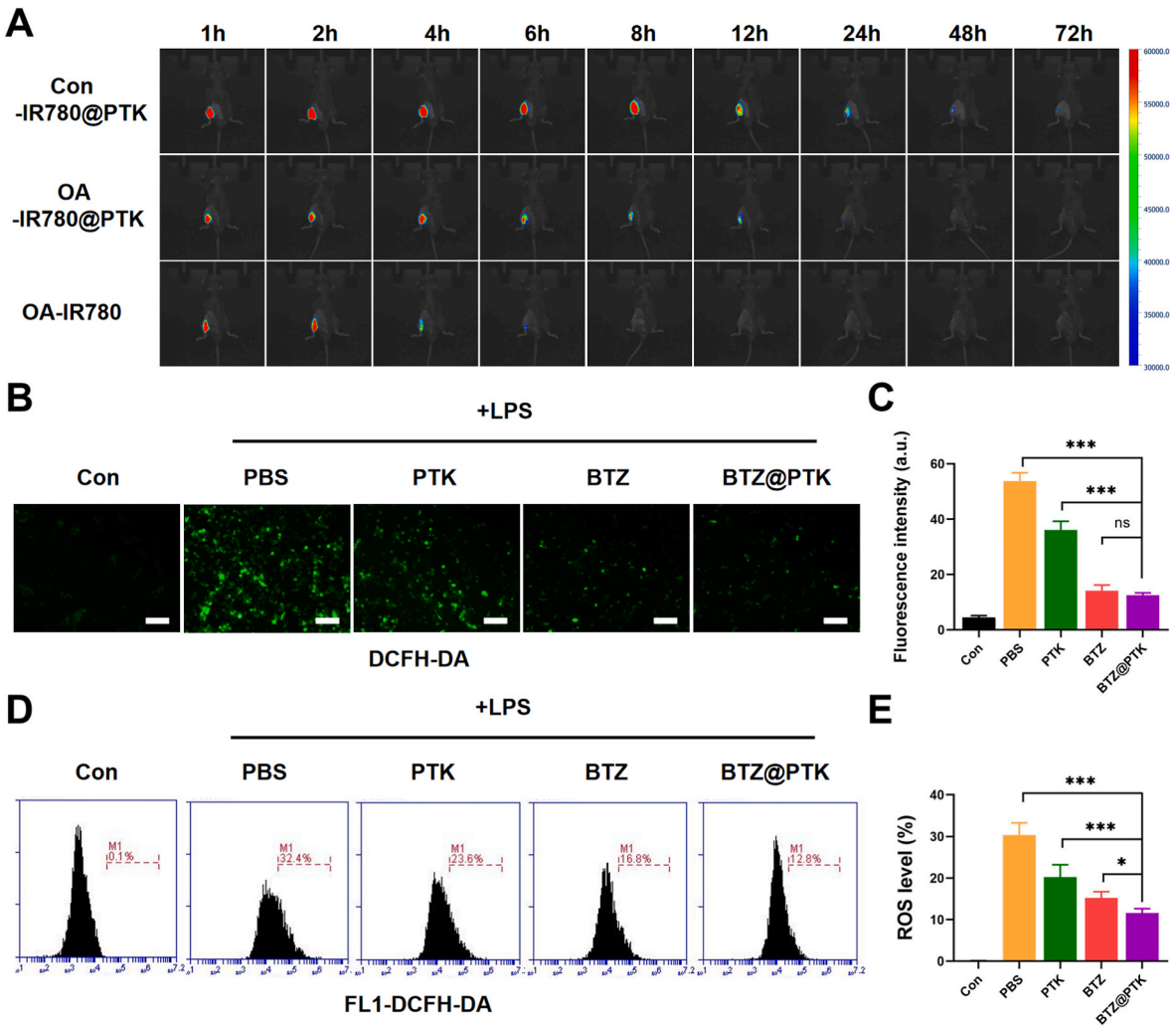

Fig. 2. Targeted biodistribution in OA mice and ROS scavenging capabilities of BTZ@PTK.
(A) Fluorescence enrichment imaging of ROS-modulated drug in inflamed vs noninflamed OA joints at different times. (B) Fluorescent images of LPS-activated RAW264.7 cells after treatment and then stained with ROS fluorescent probe DCFH-DA. Scale bar, 100 μm. (C) The quantitative fluorescence intensity of intracellular ROS in each group. (D) ROS level revealed by the fluorescence of DCFH-DA in LPS-activated RAW264.7 cells in each group by FACS. (E) Quantification of the percentage of ROS-positive cells in different groups. $^{*}P < 0.05$, $^{**}P < 0.01$, $^{***}P < 0.001$, n = 3.

high ROS level, BTZ@PTK was expected to achieve the rapid cleavage of TK linkages, which would result in the dissociation of nanoparticles and boosted release of BTZ.

The basic prepared path of ROS-responsive polymer (PTK) was illustrated in (Fig. 1A). Briefly, the precursor of thioketal linkage, carboxyl-terminal TK linker (TK-COOH), was obtained by the reaction between anhydrous 3-mercaptopropionic acid and acetone under a dry hydrogen chloride atmosphere. Subsequently, hydroxyl-terminal TK linker (TK-OH) was successfully synthesized by the reduction of TK-COOH. The chemical structure of TK-COOH and TK-OH were characterized by ^{1}H NMR spectrum (Figs. S1 and S2). Finally, ROS-responsive polymers are prepared by the coupling reaction between 1-cyanato-6-isocyanatohexane and TK-OH using monomethoxy poly(ethylene glycol) (mPEG) as the terminal capping agent. The detailed chemical structure and molecular weight of PTK were studied by ^{1}H NMR spectrum and size exclusion chromatography (SEC). As shown in Fig. S3, ^{1}H NMR spectrum of PTK demonstrated that the peaks at 3.97, 1.78, 2.60, and 1.53 ppm were assigned to protons of thioketal units. Compared with TK-OH, some new peaks appeared at 3.24, 3.51, 1.18, and 2.94 ppm in the ^{1}H NMR spectrum of PTK were attributed to the terminal methoxy of PEG and isocyanate groups, respectively. It was further proved by SEC curves that the number average molecular weight (M_n) and polydispersity index (PDI) of PTK is 28.4 kg/mol and 1.68, respectively (Fig. S4). Therefore, the amphiphilic polymer PTK containing ROS-responsive TK units was successfully synthesized.

3.2. Preparation and characterization of polymeric nanoplatform

BTZ was loaded into ROS-responsive thioketal-containing nanocarrier to form BTZ@PTK nanoparticles by the co-assembly of BTZ and PTK, which could promote the biostability of BTZ and prolong the blood circulation time of BTZ@PTK nanomedicine. As shown in the UV–vis spectra of BTZ@PTK (Fig. 1B), the characteristic absorption of BTZ at 273 nm could be observed, indicating that BTZ was encapsulated in the nanoplatform. Notably, there was a 5 nm red-shift in the absorption spectrum of BTZ@PTK compared with that of free BTZ in organic solution mainly due to the hydrophobic interaction and π-π stacking of BTZ in the hydrophobic domains of BTZ@PTK. The TEM image, shown in Fig. 1C, illustrated that the BTZ@PTK presented a spherical morphology. As shown in Fig. 1E, the hydrodynamic diameter of BTZ@PTK was ca. 120 nm. The loading content of BTZ in BTZ@PTK nanoplatform was ca. 9.1% according to the calculation based on the absorbance of BTZ in BTZ@PTK and the BTZ standard curve shown in Fig. S5.

3.3. Evaluation of ROS-responsiveness of BTZ@PTK

The ROS-responsive behavior of BTZ@PTK nanoparticles was detected by DLS and TEM analysis. Accordingly, BTZ@PTK was incubated with an extrinsic ROS source (50×10^{-3} M H_2O_2 and 1.0×10^{-6} M Fe^{2+}) for 24 h. As depicted in Fig. 1D, the thioketal linkages were broken, and the size and morphology of BTZ@PTK changed significantly. There were abundant irregular and inhomogeneous particles after the introduction of ROS solution. Particularly, some large assemblies emerged and the PDI increased from 0.15 to 0.45 after incubating with 10 mM HClO solution (Fig. 1E). In addition, as shown in Fig. 1F, similar results were found when the nanoparticles were co-incubated with and 1.0 mM H_2O_2. Therefore, the above data indicated that BTZ@PTK possessed predominant ROS-responsive performance.

Some previous research works reported that the ROS concentration of human OA synovial fluid was 2–5 folds higher than that in normal synovial fluid (ca. 100–200 μM) [28,29]. We have collected 3 samples of human OA synovial fluid and studied the ROS responsiveness of the nanomedicine. 9,10-Diphenyl anthracene (An) was used as the fluorescence probe of ROS responsiveness in human OA synovial fluid. As shown in Fig. S6, the fluorescence intensity in human OA synovial fluid was much lower than that in PBS, since the high ROS levels in human OA synovial fluid resulted in the breakage of PTK and the release of An. The aggregation of released An led to the dropdown of fluorescence intensity at 430 nm. Thus, the comparison study confirmed the ROS-responsiveness of BTZ@PTK in human OA synovial fluid.

3.4. Drug release behavior in an inflammatory microenvironment in vitro

Having certified the ROS-responsiveness of the BTZ@PTK nanomedicine, the *in vitro* drug release behavior was investigated. After being stimulated by 1.0 mM H_2O_2, BTZ can be effectively released. As shown in Fig. 1G, around 60 % of loaded BTZ could be released while mixed with 1.0 mM H_2O_2 solution for 24 h. However, the negligible release of BTZ was observed in the absence of H_2O_2 solution. It further established that the release rate of BTZ could be extremely accelerated by the high level of ROS, illustrating that the release of BTZ would be much higher in OA joints than that in normal tissues because of the overexpressed ROS in OA inflammatory joints.

3.5. Targeted biodistribution of nanoparticles in inflammatory joints of OA mice

Recently, fluorescence imaging has been demonstrated to be a valuable tool for observing biological distribution with high resolution [30]. To further address the *in vivo* accumulation and distribution of nanoparticles during the whole procedure in the inflammatory joints, IR780 (a NIR cyanine dye) or PTK co-assembling IR780 (named IR780@PTK) was used to inject into joints of DMM-induced OA mice, serving as representations of free drug and nanomedicine, respectively. In the control group, only IR780@PTK was injected to examine the biodistribution patterns of drug release in non-inflamed joints. The dynamics of IR780 fluorescence over the joint were visualized at 1, 2, 4, 6, 8, 12, 24, 48 and 72 h after injection among three groups. We found that the fluorescence intensity from normal joints injected IR780@PTK with strong signals within 8 h, then gradually decreased and almost removed completely by 72 h, suggesting nanoparticles exhibit weak emission in the non-inflamed tissues. In contrast, in OA joints, the fluorescence signal in the free IR780 group vanished swiftly following 6 h whereas the fluorescence intensity in IR780 @PTK group decreased gradually from 1 h to 24 h and was completely removed after 24 h. These findings imply that the nanoplatform not only targets at inflammatory sites but also offers a stable long-term accumulation in this microenvironment (Fig. 2A and **S7)**. Furthermore, at 24 h after injection, the organs (liver, heart, spleen, lungs, and kidneys) and limbs of mice from each group were collected to assess the circulation of nanomedicine. Compared to that in normal joints, the fluorescence signals in IR780 @PTK group after OA surgery was particularly strong in the limb in OA joints and partially enriched in the organs of liver, kidney, and lungs (Fig. S8), indicating that the nanoparticles preferentially targeted the inflamed joints and primarily metabolism through the liver, lung, and kidney.

3.6. Evaluation of ROS scavenging ability in vitro

During the OA progression, the level of intracellular ROS secreted by inflammatory synovial tissues regularly increased, leading to a high level of matrix metalloproteinase, which triggered chondrocyte apoptosis and cartilage degradation [31,32]. Thus, scavenging overproduced ROS in inflamed joints will be beneficial for OA treatment. Prior to investigate the intracellular ROS elimination ability of BTZ@PTK, the cytotoxicity against RAW 264.7 cells was determined by CCK-8 assay. For comparison, the cell viability was not significantly affected by BTZ@PTK after the incubation for 24 h and 48 h at the BTZ concentrations ranging from 0.25 to 1 nM, and there was no significant distinction among the PTK, BTZ and BTZ@PTK groups, indicating satisfactory biosecurity of BTZ@PTK (Fig. S9). Moreover, in order to examine the effect of nanomedicine on normal tissue cells, the toxicity of BTZ@PTK against the primary chondrocytes and osteoblastic MC3T3-E1 cells were detected by CCK-8 assay. The results found that both cells treated with or without PTK, BTZ, and BTZ@PTK (0.25, 0.5, and 1 nM) has no significant variations in cell activity among groups (Figs. S10 and S11), implying that at concentrations ranging from 0.25 to 1 nM, BTZ@PTK may have little effect on chondrocytes and osteogenesis.

Furthermore, the *in vitro* ROS scavenging activity of BTZ@PTK was investigated utilizing LPS-activated RAW264.7 macrophages. LPS can induce an inflammatory response in RAW264.7 cells in a created environment with overexpressed ROS [33]. Therefore, we employed RAW264.7 cells activated with LPS and treated with PBS, PTK, BTZ and BTZ@PTK, respectively, and intracellular ROS generation was measured using a fluorescent probe, 2′,7′-dichlorodihydrofluorescein diacetate (DCFH-DA). In the result, a noticeable rise in ROS signals was observed in PBS group following LPS stimulation, which approximately increased 10-fold of fluorescence intensity compared to those without LPS stimulation, suggesting there was an excess of ROS in the inflammatory response. However, both free medication BTZ and BTZ@PTK therapy had benefits in scavenging ROS, while BTZ@PTK exhibited the stronger effect. BTZ@PTK could significantly suppress fluorescence intensity of ROS to 23.3% compared with the PBS group without BTZ@PTK treatment. In addition, the drug carrier PTK also contributes to the inhibition of ROS generation at the BTZ equal concentration of 1×10^{-6} M (Fig. 2B and C). It might be related to ROS-induced nanoparticle dissociation, which caused by the cleavage of TK units, consuming some of the ROS content and thereby decreasing ROS levels. Thus, these findings suggested that BTZ@PTK would show an immediate respond to the ROS-rich microenvironment and exert synergistic effect against the excessive ROS in OA inflamed joints.

Furthermore, the similar results can also be found in ROS scavenging assay by flow cytometry. Among PTK, BTZ and BTZ@PTK three groups, BTZ@PTK also showed the greatest ability to scavenge ROS and inhibit the numbers of ROS-positive cells to approximately 38.2% compared with the PBS group (Fig. 2D and E). These results suggested that BTZ@PTK exhibited a competent reduction in ROS overconditioning, exerting a beneficial effect against inflammatory microenvironment.

3.7. Anti-inflammatory effect of BTZ@PTK in vitro

During the classical inflammatory reactions, macrophages particularly operate as potent effector cells, and can be broadly sorted into classic (M1) and alternative (M2) two subsets in response to different stimuli from their microenvironment, performing pro-inflammatory and anti-inflammatory functions, respectively [34]. Activation of M1 macrophages can be induced by LPS stimulation or interferon-γ (IFN-γ),

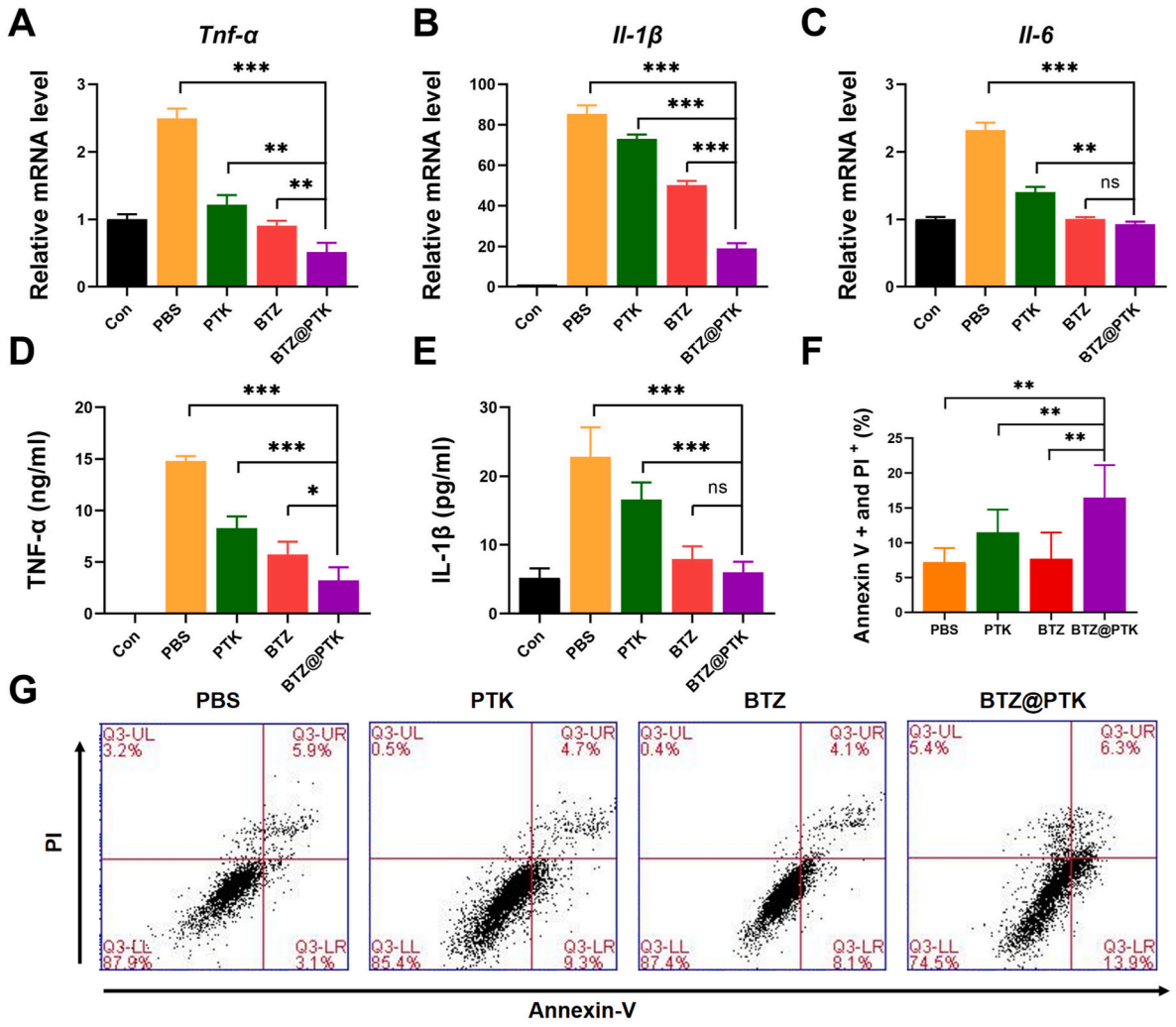

Fig. 3. Effect of BTZ@PTK on anti-inflammatory and M1 macrophage apoptosis in LPS-activated RAW264.7 cells.
Expression of M1 macrophage markers TNF-α (A), IL-1β (B) and IL-6 (C) were examined by qPCR, 18s was used as internal reference gene. The levels of cytokines TNF-α (D) and IL-1β (E) in the supernatants of LPS-activated RAW264.7 macrophages cultures were determined by ELISA. (F) The percentage of early apoptotic (Annexin V+/PI-) cells plus the percentage of late apoptotic (Annexin V+/PI+) cells. (G) The apoptosis of the activated RAW 264.7 cells after various treatments within 24 h. Data are represented as mean ± SD, $^{*}P < 0.05$, $^{**}P < 0.01$, $^{***}P < 0.001$, n = 3.

while the polarization of M2 macrophages can be activated by IL-4 and/or IL-13 [35]. In OA joints, macrophages are predominantly of the M1 phenotype, which secret a large amounts of inflammatory cytokines such as TNF-α, IL-1β and IL-6, which leading to joints injury [9]. Thus, we used the LPS-stimulated macrophages to evaluate the anti-inflammatory capability of nanomedicine for reprogramming M1 response. Compared to the PBS-treated cells, BTZ@PTK significantly decreased the mRNA expression of TNF-α, IL-1β and IL-6 in LPS-activated RAW264.7 cells. The inhibitory capacity of BTZ@PTK in blocking TNF-α and IL-1β was found to be more pronounced when compared with the BTZ-treated groups (Fig. 3A–C). Subsequently, the protein expression levels of TNF-α and IL-1β were validated by ELISA. Consistent with the qPCR results, BTZ@PTK treatment could reduce the pro-inflammatory cytokines TNF-α and IL-1β levels to one quarter compared with the non-treated control (Fig. 3D and **E**). These results showed that BTZ@PTK could exert an effective anti-inflammatory activity by modulating M1 macrophage polarization, and subsequently regulating inflammation cytokines expression.

To better understand the anti-inflammatory effect of BTZ@PTK, the Annexin V/PI assay for the extent of cell death was evaluated against the LPS-treated RAW264.7 cells. In comparison to the activated macrophages in the PBS group, the treatment of 1.0 nM BTZ@PTK showed a 3-fold boost of the proportion of apoptotic cells after 24 h incubation, whereas the free drug had no discernible effect on cell apoptosis. Moreover, it was interesting to discover that the group of polymeric nanocarrier PTK also exhibited an increase in apoptosis for the polarized M1 macrophages (Fig. 3F and **G**). On the contrary, the PTK and BTZ@PTK had no obvious effect on the viability of normal macrophages (Fig. S9). These results investigated that BTZ@PTK might have selective toxicity towards the inflammatory cells against the normal macrophages, indicating that the high biosafety of BTZ@PTK would lead to negligible side effects in the normal tissues.

Previous studies have proven that the excessive ROS in the inflamed joints induced synovial inflammation and M1 macrophage activation [12,36]. In our results, we found BTZ@PTK not only acted as a ROS scavenger to down-regulate the ROS level but also caused the M1 macrophage apoptosis. These results illustrated that the inflammatory microenvironment played an essential role in the modulation of synovial inflammation. Since the activated M1 macrophage is pathologically featured with high oxidative pressure, the scavenge of ROS by nanomedicine significantly remodeled the OA microenvironment including but not limited to the ROS level, inflammatory cytokines, and even the M1 macrophage apoptosis. The ROS regulation activity of BTZ@PTK is mainly controlled by intracellular ROS level. Collectively, the BTZ@PTK

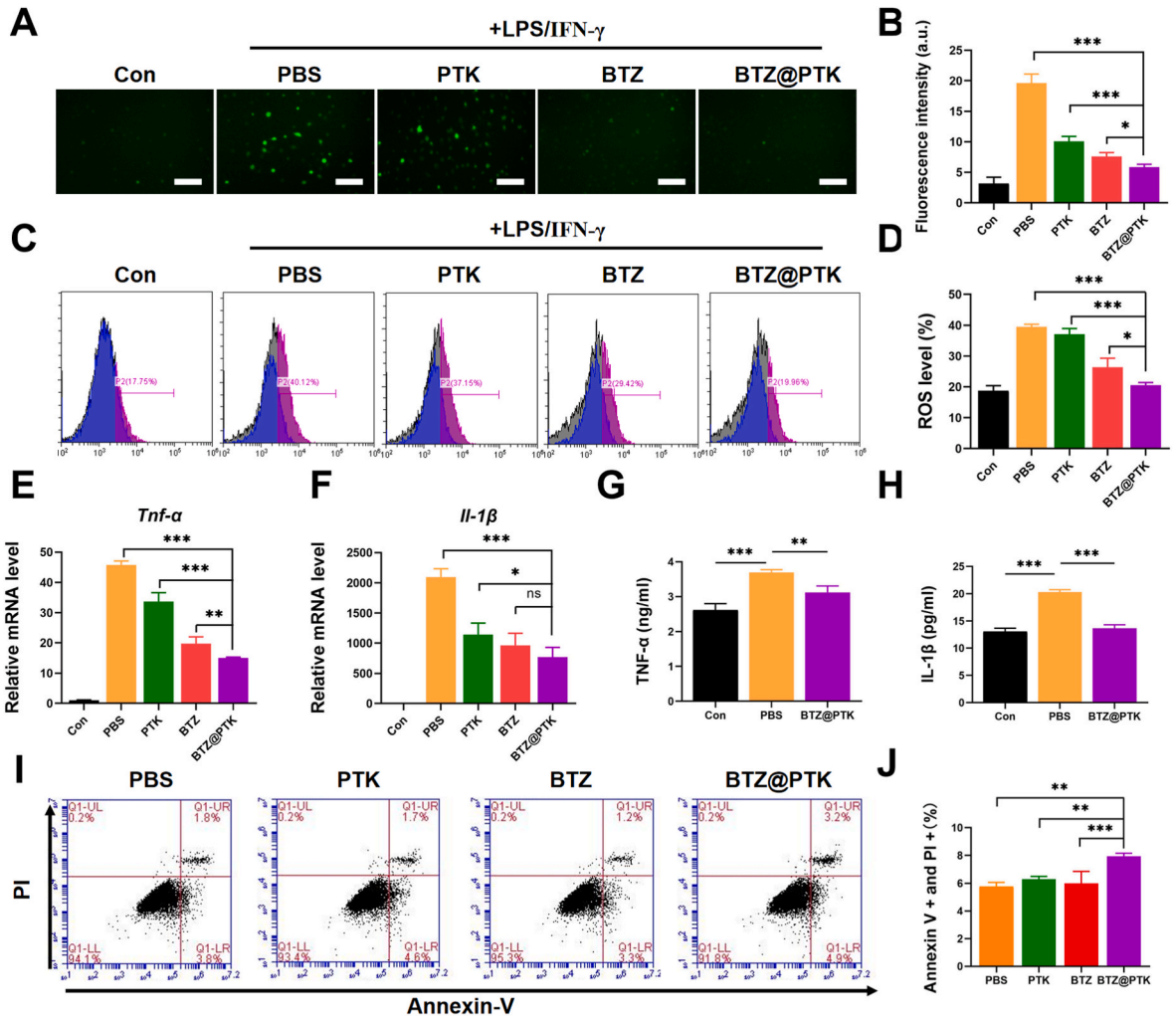

Fig. 4. Effect of BTZ@PTK on modulation of the inflammatory microenvironment in LPS/IFN-γ-stimulated primary macrophages.
BMDMs isolated from WT mouse tibiae and femora and were cultured with M-CSF for 5 days to generate bone marrow macrophages. Then cells were treated with or without LPS (1 μg/mL)/IFN-γ (100 ng/mL) for 6 h followed by treatment with PBS, PTK, BTZ, BTZ@PTK (1 nM) for another 24 h. (A) Representative immunofluorescence images of LPS/IFN-γ-stimulated primary macrophages stained with ROS fluorescent probe DCFH-DA. Scale bar, 100 μm. (B) Quantification of the percentage of ROS positive cells in different groups. (C) ROS level revealed by the fluorescence of DCFH-DA in LPS/IFN-γ-stimulated primary macrophages in each group by FACS. (D) Quantitative the fluorescence intensity of intracellular ROS in each group. (E) Expression of M1 macrophage markers TNF-α (E), IL-1β (F) were examined by qPCR, 18s was used as internal reference gene. The levels of cytokines TNF-α (G) and IL-1β (H) in the supernatants of LPS/IFN-γ activated M1 macrophages cultures were determined by ELISA in the Con, PBS, and BTZ@PTK groups. (I) The percentage of early apoptotic (Annexin V+/PI-) cells plus the percentage of late apoptotic (Annexin V+/PI+) cells. (J) The apoptosis of the M1 macrophage after various treatments within 24 h. Data are represented as mean ± SD, $^{*}P < 0.05$, $^{**}P < 0.01$, $^{***}P < 0.001$, n = 3–4.

could precisely suppress inflammatory response with little effect on the non-inflamed tissues.

3.8. Effect of BTZ@PTK on ROS scavenging and anti-inflammatory activities of BM macrophages

In order to better understand the effect of BTZ@PTK on the macrophages, we further analyzed the effect of BTZ@PTK on ROS scavenging and anti-inflammatory activities in primary macrophages. BMDMs were isolated from WT mouse tibiae and femora and were cultured with M-CSF for 5 days to generate BM macrophages. On day 5, cells were treated with or without 1 μg/mL of LPS plus 100 ng/mL of IFN-γ for 6 h followed by treatment with PBS, PTK, BTZ, BTZ@PTK (1 nM) for another 24 h. Consistent with the results of RAW264.7 cells, in the LPS/IFN-γ treated primary macrophages, BTZ@PTK also could block the increased ROS generation, inhibit the high levels of inflammatory cytokines TNF-α and IL-1β and induce the M1 macrophages apoptosis (Fig. 4). These findings suggest that BTZ@PTK has potent ROS scavenging and anti-inflammatory capabilities.

Similarly, apoptosis assay showed that the free drug of BTZ under the concentration of low dose (1 nM), had no obvious pro-apoptotic effect on M1 macrophages after 24h treatment, while the BTZ@PTK had selective toxicity towards the M1 macrophages. According to the findings of *in vivo* (Fig. S7) experiments, it is confirmed that the nanomedicine could be controlled release of BTZ specifically in inflammatory tissue, and maintained much more time in the inflammatory microenvironment than the free BTZ, illuminating that the effect time of nanomedicine on inflamed RAW264.7 cells or primary macrophages was significantly longer in the BTZ@PTK groups, which may be the explanation for the nanomedicine triggering M1 macrophage apoptosis.

3.9. Therapeutic effects of BTZ@PTK on OA-related symptoms

After confirming the excellent anti-inflammation efficiency of BTZ@PTK *in vitro*, the *in vivo* performances were studied using the destabilization of the medial meniscus (DMM)-induced OA model. DMM

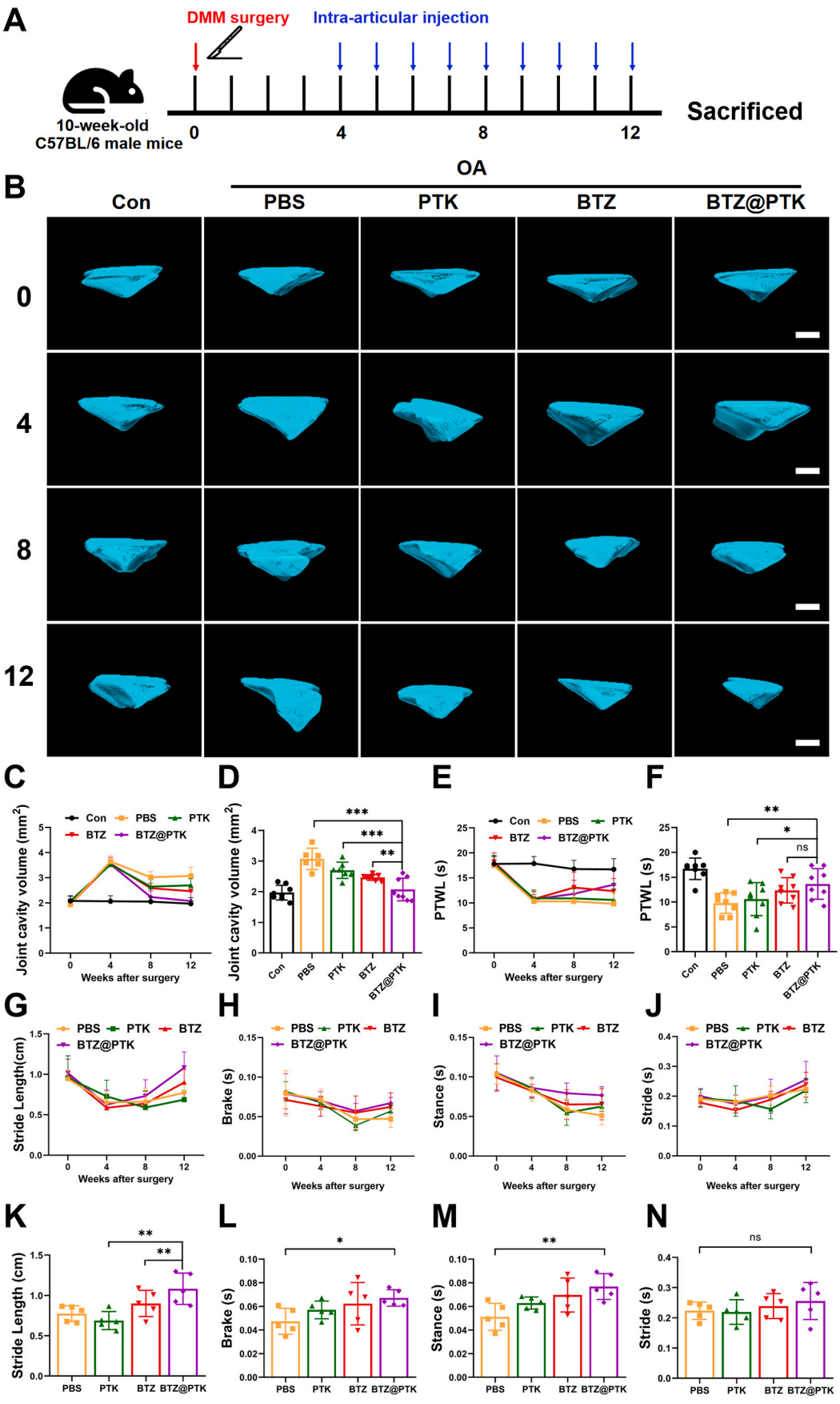

(caption on next page)

Fig. 5. Effect of BTZ@PTK on OA-related symptoms.
(A) Illustration of the experimental schedule against DMM-induced OA model in mice. (B) 3D reconstruction of the joint space volume in 0, 4, 8, 12 weeks post-OA surgery. Scale bar, 100 μm. (C) Joint cavity volume in different times, n = 6–8. (D) Joint cavity volume in different group at 12 weeks post-OA surgery times, n = 6–8. (E) PWTL was tested at the right hind paw of different groups, n = 6–8. (F) PWTL at 12 weeks post-OA surgery, n = 6–8. Gait analysis was performed by DigiGait imaging system and the right hind limb was chosen as the observation index. (G) Stride length (cm), (H) Brake (s), (I) Stance (s) and (J) Stride (s)in different times. (K) Stride length (cm), (L) Brake (s), (M) Stance (s) and (N) Stride (s) at 12 weeks post-OA surgery times in each group, n = 5. The data are presented as means ± SD. $^{*}P < 0.05$, $^{**}P < 0.01$, $^{***}P < 0.001$.

model is one of the most well-established and widely used OA models, which is closely similar to human OA in pathologic features [22]. Therefore, DMM surgery was performed on 10-week-old C57BL/6 mice, and after 4 weeks of treatment with PBS, PTK, BTZ and BTZ@PTK for consecutive 8 weeks by intra-articular (i.a.) injection per week, normal mice as the control. The severity of synovitis and OA-related symptoms were evaluated before (baseline) and at weeks 4, 8, and 12 after the surgery. For instance, knee ultrasonography was subjected to collect and quantify the synovial abnormalities and PTWL was used to evaluate the pain behavior, as well as the rotarod test and gait analysis to identify joint coordination (Fig. 5A).

It is known that the volume of synovial tissue increased during OA progression, and synovial hyperplasia was significantly correlated with increased synovial inflammation [23]. Consistently, the joint space volume was dramatically enhanced at all times after OA surgery. Compared to the control, the amount of synovial tissue in OA mice reached its peak at 4 weeks, expanded almost 1.5-fold, thereafter dropped slightly at 8 weeks, and remained stable until 12 weeks, indicating persistent synovitis in the development of OA pathology. Intra-articular administration of BTZ@PTK can reduce synovial hyperplasia for greater efficacy with a significant time-dependent decrease of joint gap volume, in particular, at 12 weeks approximating that of normal mice (Fig. 5B–D), suggesting the BTZ@PTK had a great ability to reduce synovial inflammation with a time-dependent curative effect.

Furthermore, chronic inflammation will continuously stimulate to nociceptors leading to thermal pain hypersensitivity [37]. OA is generally classified as nociceptive (inflammatory) pain. In order to quantify the nociceptive threshold in OA model, we measured PTWL in different groups using a thermal pain stimulator. In common, lowered PTWL equates to higher pain. To our satisfaction, BTZ@PTK treatment

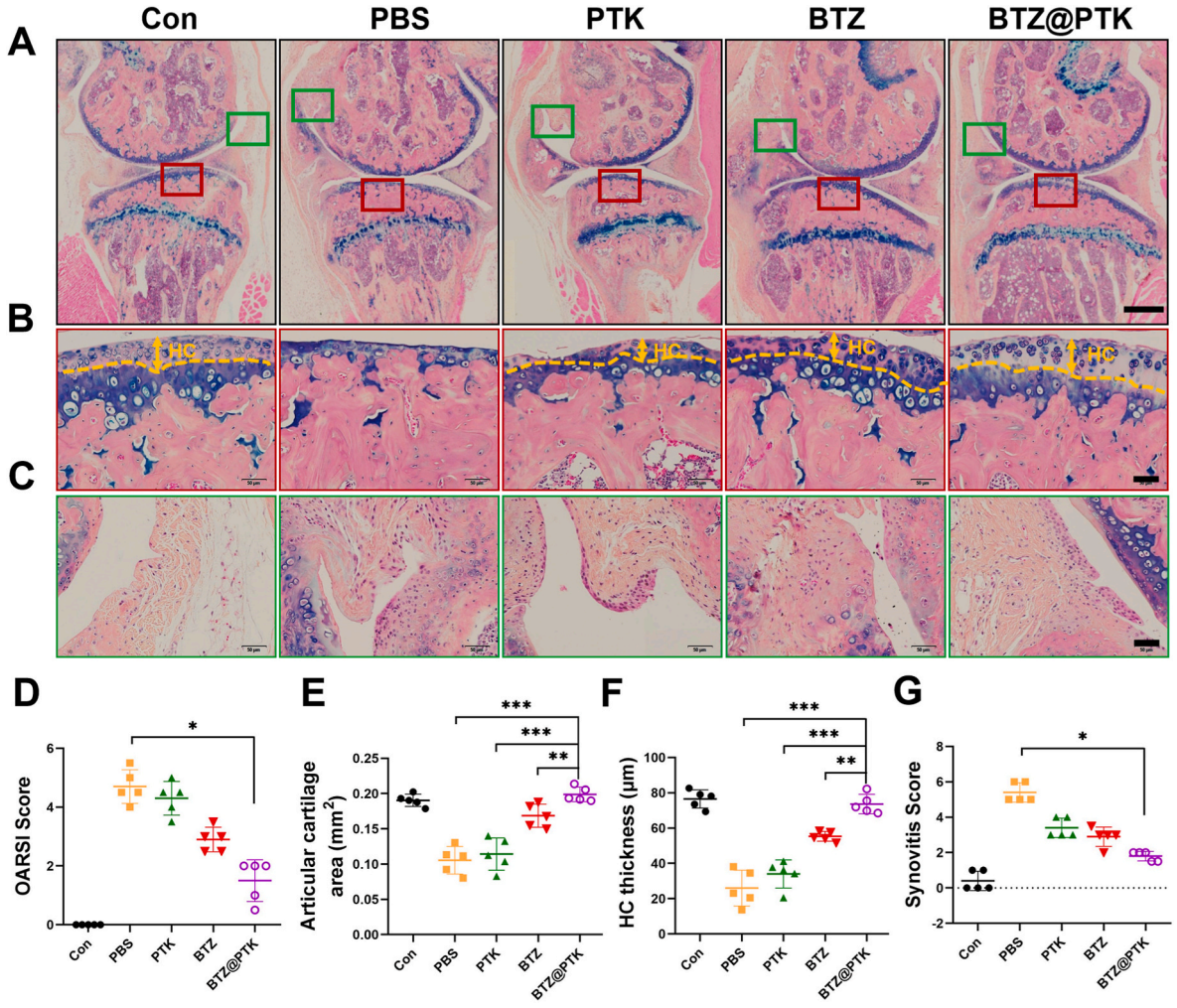

Fig. 6. Effect of BTZ@PTK on synovitis and cartilage degradation of OA model.
(A) Pathological staining of knee joints with ABOG staining. Scale bar, 500 μm. Cartilage (B) and synovium (C) with ABOG staining. Scale bar, 50 μm. (D) OARSI, Osteoarthritis Research Society International. The OARSI score was graded to the medial tibial plateau in different groups. (E) The articular cartilage areas in different groups. (F) The thickness of hyaline cartilage (HC) was indicated by double arrows. (G) The synovitis score was presented in different groups. Scale bar, 50 μm $^{*}P < 0.05$, $^{**}P < 0.01$, $^{***}P < 0.001$, n = 5.

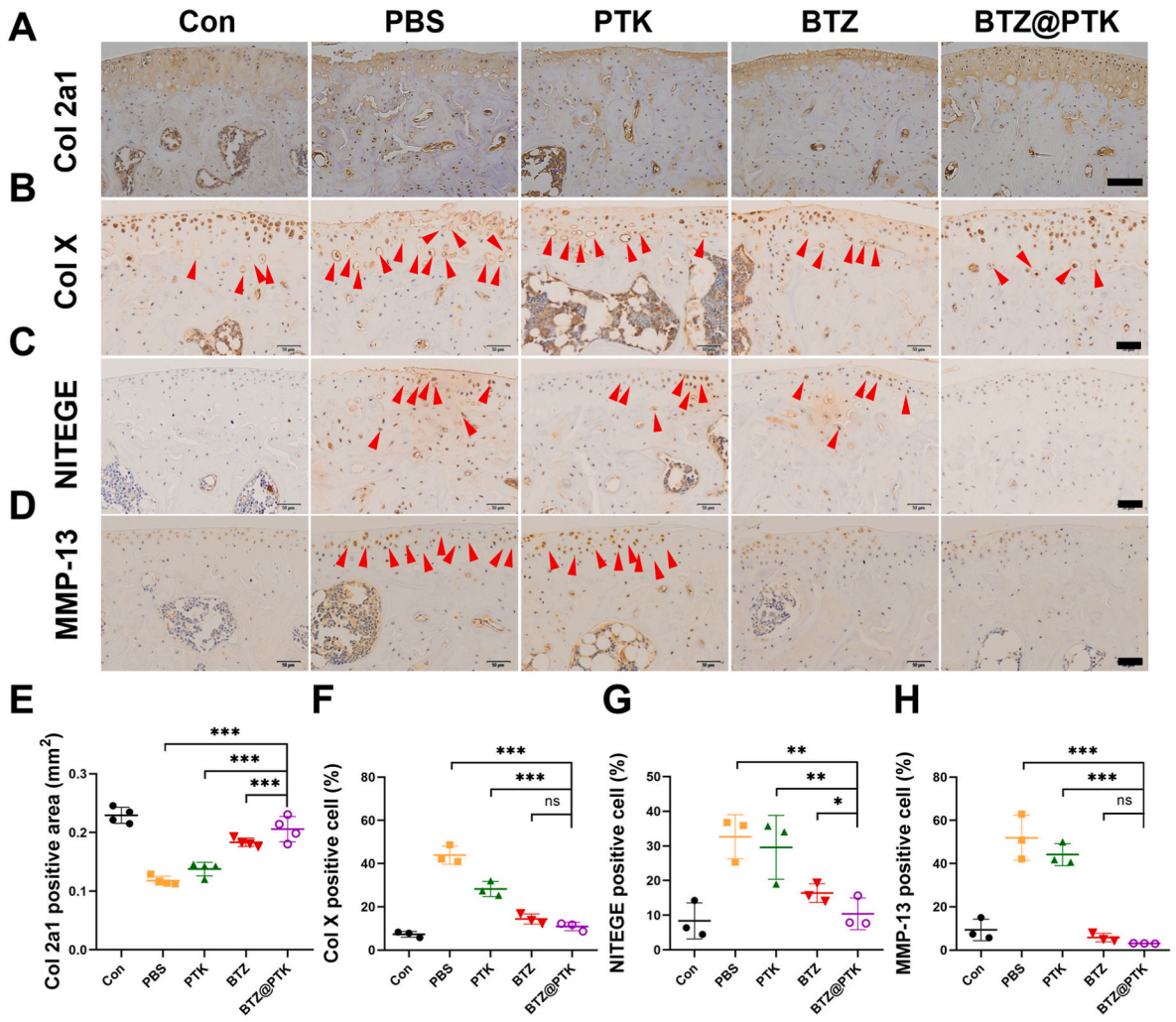

Fig. 7. Effects of BTZ@PTK on expressions of Col 2a1, Col X, NITEGE and MMP-13 of cartilage in OA model.
(A) IHC staining of Col 2a1. Scale bars, 100 μm. IHC staining of Col X (B), NITEGE (C) and MMP-13 (D) of cartilage in OA mice. Scale bars, 50 μm. (E) Quantitative analysis of articular cartilage areas in the knee joints. Quantification analysis the number of Col X-positive cells (F), MMP-13-positive cells (G), and NITEGE-positive cells (H) in each group. $^{*}P < 0.05$, $^{**}P < 0.01$, $^{***}P < 0.001$, n = 3–4.

produced a pretty long relief of thermal hyperalgesia of DMM-induced OA mice (Fig. 5E and **F**), which was consistent with the effect of persistent synovitis inhibition, suggesting BTZ@PTK could ameliorate chronic pain in OA models by suppressing chronic synovitis. Therefore, we believe that BTZ@PTK may be a potential therapeutic strategy for inflammatory pain in arthritis.

In clinic, chronic pain in OA patients commonly affects joint function causing difficulty in walking and altered gait biomechanics [38]. Animal experiments also have been reported gait disruption in DMM-induced OA mice [39]. To determine whether BTZ@PTK alleviates the gait disturbance in OA development, we used gait analysis to get the performance with monthly assessments. In the result, at 4 weeks after OA surgery, the mice showed severe gait abnormalities with shortened stride length, stride, brake and stance, suggesting OA mice became walk slowly, BTZ@PTK therapy improved the slower gait velocity, but with little function on the stride (Fig. 5G-N). Moreover, BTZ@PTK increased OA-induced impaired rotarod performance at 12 weeks after treatment, however, there were no significant variations in rotarod latency fall time across groups (Fig. S12). In brief, these results revealed that BTZ@PTK treatment could partially improve the function of the knee joint and alleviate the gait patterns of DMM-triggered OA mice.

3.10. Effect of BTZ@PTK on osteoarthritic changes in synovium and cartilage

The pathological changes of synovium and cartilage are the main focus of the characteristics of osteoarthritic changes. Normal synovium has two layers: one is the intimal lining layer, which contains 1–2 cells thickness of macrophages and fibroblast-like synoviocytes, and the other is the synovial sublining layer, which is made up of scattered blood vessels and fibroblasts with few lymphocytes or macrophages [40]. The main morphological hallmark of synovitis is the accumulation of macrophage lines in the synovium's intimal lining [41,42]. Besides, OA microenvironment primarily drives the degeneration and fibrosis of articular cartilage. Therefore, we evaluated pathological changes in synovium and cartilage histologically following Alcian blue/-Hematoxylin/Orange G (AB/OG) staining. The cartilage was detected by Alcian blue staining, whereas the bone was revealed by Orange G. In the control group, the surface of articular cartilage presented smooth and maintained integrity, however, 12 weeks after OA surgery, articular cartilage exhibited Alcian blue loss mostly and fibrillation in joints with an OARSI score of 4.70 ± 0.57. In the BTZ@PTK group, the defected surface presented more smoothly and the regenerated tissue appeared similar to the native cartilage with a significantly lower OARSI score (1.50 ± 0.70) (Fig. 6A, B and **D**). Notably, the articular cartilage areas in

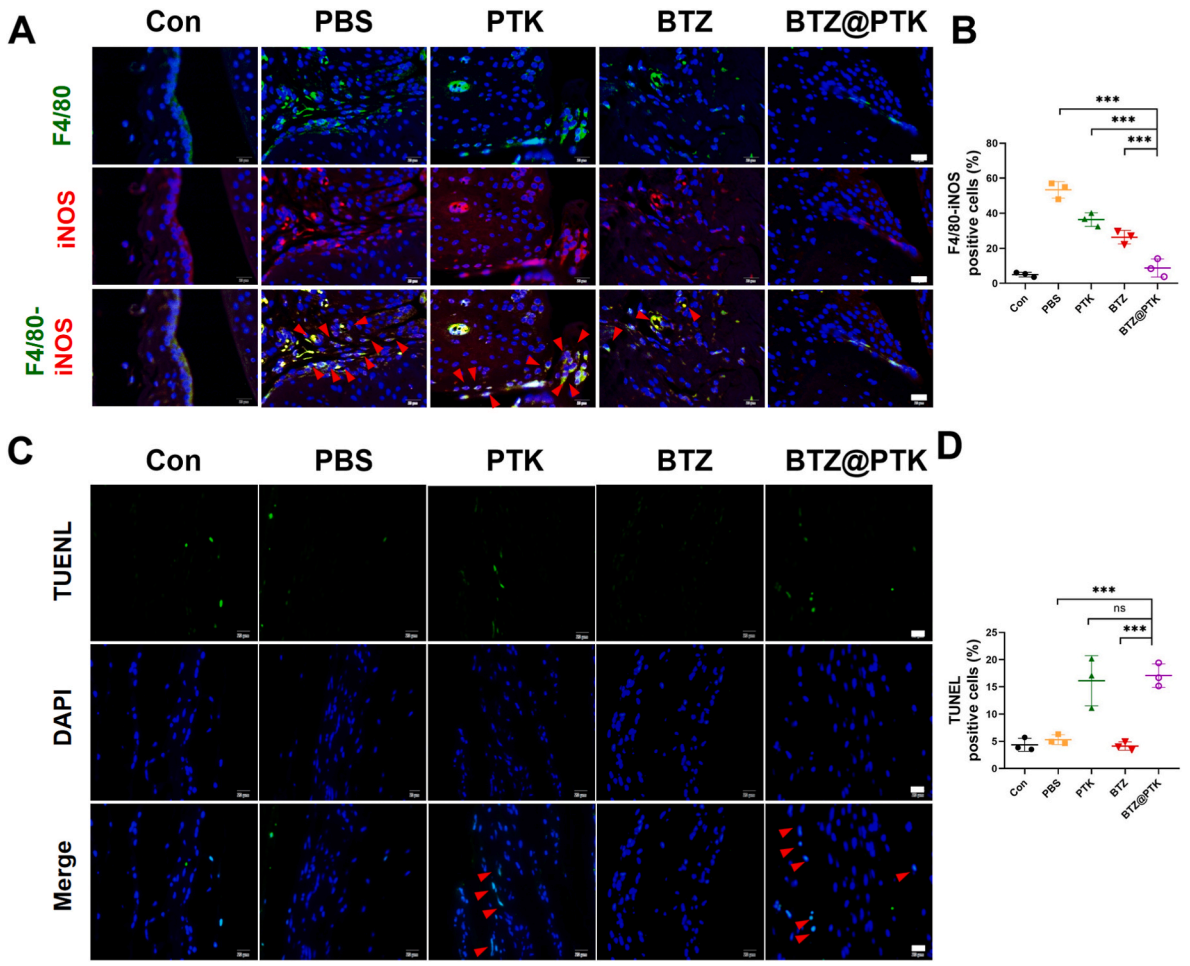

Fig. 8. Effect of BTZ@PTK on M1 phenotype and macrophage apoptosis in synovium.
(A) Representative images of coimmunostaining for pan-macrophages (F4/80^{+}, green) plus M1 marker (iNOS^{+}, red) in synovium in the different groups. Scale bar, 20 μm. The red arrow represents the positive F4/80-iNOS^{+} cells. (B) Quantitative analysis of F4/80-iNOS-positive macrophages compared with total macrophages. (C) TUNEL staining of the synovium in different groups. Scale bar, 20 μm. (D) Quantitative analysis of positive apoptosis macrophages in the synovium. ***$P < 0.001$, n = 3–4.

the tibia were improved by BTZ@PTK treatment (Fig. 6E). Furthermore, the thickness of the hyaline cartilage (HC) layer decreased with tidemark moving closer to the articular surface in OA group whereas BTZ@PTK reversed this tendency (Fig. 6F). Safranin O/Fast green (SO/FG) staining were further assessed to detect the cartilage damage and changes in aggrecan levels. The result showed the aggrecan expression as indicated by red staining was significantly reduced in OA mice compared to controls, while BTZ@PTK remarkedly restored the loss of aggrecan expression (Fig. S13), indicating BTZ@PTK provided efficient cartilage protection in OA models. Thus, BTZ@PTK protects articular cartilage by reversing the HC thickness, OARSI score and aggrecan level.

Consistent with previous results [8,43], our study found that synovial tissue in OA became proliferative and hypertrophic with abundant cell infiltration in the lining and sublining layer, along with higher synovitis scores than that of normal controls, but there was little proliferation in the synovium of BTZ@PTK (Fig. 6C). The synovitis scores were in order of BTZ@PTK < BTZ < PTK < PBS (Fig. 6G). The level of synovial inflammation is closely linked to the synovial score [23]. In the result, the mice treated with BTZ@PTK displayed a significantly lowered synovitis score, indicating the least amount of inflammation among the treatment groups. Collectively, these findings provide evidence that the application of BTZ@PTK greatly alleviated OA changes in cartilage degradation and effectively inhibited synovial inflammation.

3.11. Effects of BTZ@PTK on cartilage matrix metabolism

Chondrocytes secrete collagens, elastin, proteoglycans and other extracellular matrix (ECM) components. The majority of cartilage ECM is composed of Col 2a1 and aggrecan, and it protects the integrity of bone and maintains cartilage tension and compressive properties [44]. In OA joints, the disordered chondrocytes down-regulated the protein level of Col 2a1 and up-regulated expression of Col X and matrix metalloproteases (MMPs) [45–47]. Importantly, overexpression of MMP-13 degrades Col 2a1 in cartilage, leading to resultant joint destruction [48,49]. Besides, the expression of NITEGE, an ACAN neoepitope antibody, mediates cleaved aggrecan on the cartilage sections. Therefore, to examine whether BTZ@PTK affects the chondroprotective potential, we performed IHC staining for Col 2a1, Col X, MMP-13 and the NITEGE to detect synthesis and degradation of the cartilaginous matrix. In the results, osteoarthritic chondrocytes had reduced anabolic genes Col2a1 and increased production of catabolic genes, including Col X, NITEGE and MMP-13. After treatment with different drugs, BTZ@PTK significantly prevented the overexpression of Col X, NITEGE and MMP-13, meanwhile, rescuing the cartilage matrix loss in OA chondrocytes (Fig. 7A–D). The Col2a1-associated areas of the articular cartilage at 12 weeks following OA surgery were significantly reduced compared to controls, and BTZ@PTK therapy had a remarkable effect on cartilage protection, even recovering to the level of the normal condition (Fig. 7E). In addition, as compared to PBS-treated OA mice, BTZ@PTK

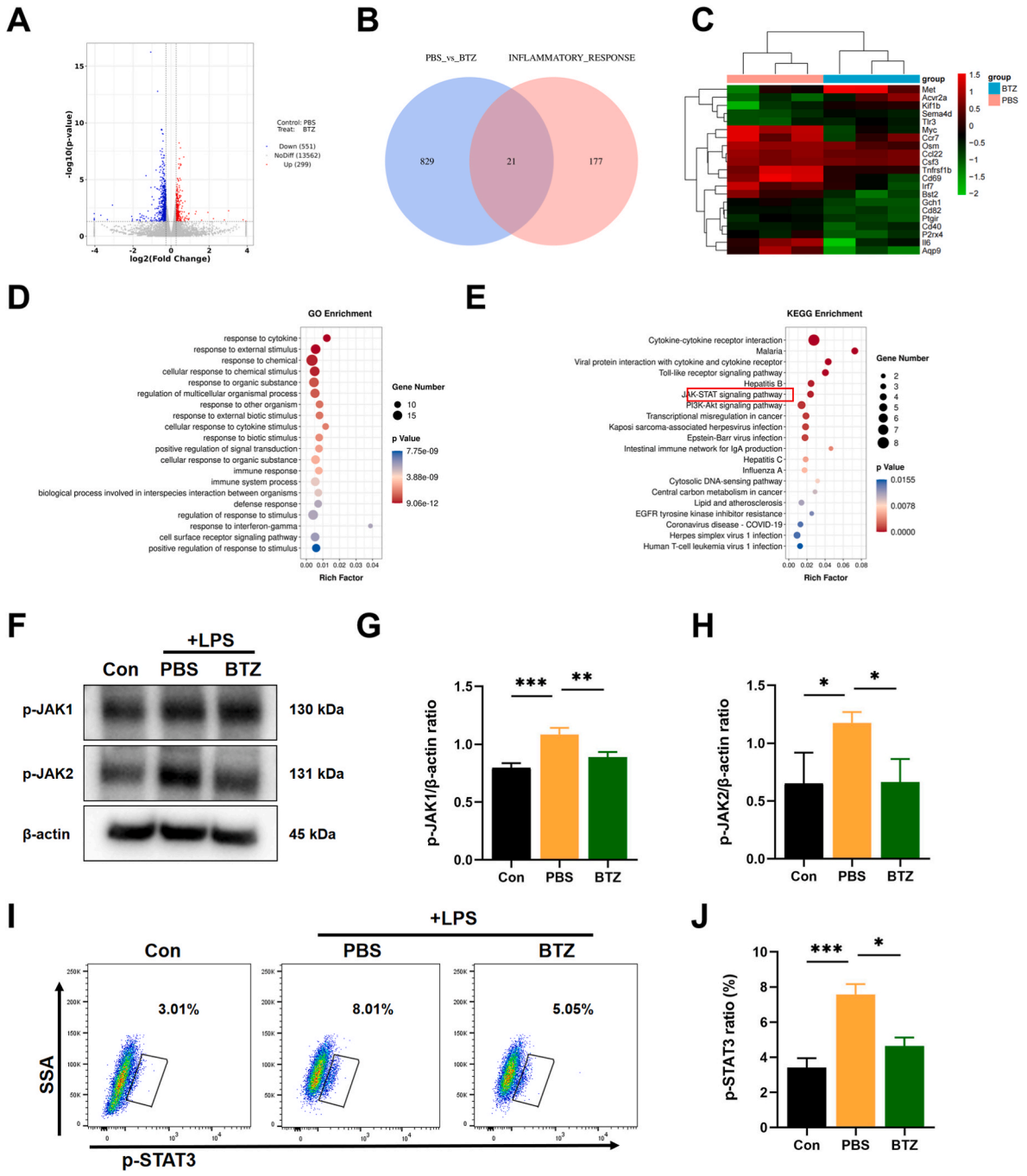

Fig. 9. Transcriptomic analysis of BTZ treatment in LPS-induced inflammatory response.
(A) Volcano plot representation of differentially expressed genes between PBS and BTZ group (adjusted 1.5 fold, p-value <0.05). (B) Venn diagram of depicting intersecting genes of PBS vs BTZ and inflammatory-related genes database. (C) Heatmap showing differential gene expression in 21 intersected genes of PBS/BTZ and inflammatory-related genes database. (D, E) Functional characterization against 21 intersected genes of PBS/BTZ and inflammatory-related genes database. (F) RAW 264.7 cells were stimulated with LPS (1 μg/mL) in the presence or absence of BTZ (1 nM) treatment for 2 h. Total cellular proteins were collected to detect the p-JAK1 and p-JAK2. β-actin served as a loading control. (G) Quantification of expression levels of p-JAK1 protein. (H) Quantification of expression levels of p-JAK2 protein. (I) RAW 264.7 cells were stimulated with LPS (1 μg/mL) in the presence or absence of BTZ (1 nM) treatment for 2 h, the expression of p-STAT3 in each group was detected by flow cytometric analysis. (J) Quantification of the percentage of p-STAT3 in each group. The data are presented as the mean ± SD. $^{*}P < 0.05$, $^{**}P < 0.01$, $^{***}P < 0.001$, n = 3.

had a substantial effect on downregulating the levels of Col X, NITEGE, and MMP-13 over consecutive 8 weeks of therapy, with the proportion of positive cells lowered to approximately 30%, 30%, and 50%, respectively (Fig. 7F–H). To summarize, BTZ@PTK treatment could recover the metabolic disturbance in the ECM of DMM-induced OA model, including increased Col 2a1 and inhibited the expression of Col X, NITEGE and MMP-13.

3.12. Effect of BTZ@PTK on macrophage M1 phenotype and apoptosis in synovuim

To explore the mechanism underlying the delayed progression of cartilage matrix catabolism in BTZ@PTK-treated OA model, we examined changes in the phenotypic alteration of synovial M1 macrophages in OA joints by immunofluorescence staining of M1 (iNOS, red) markers.

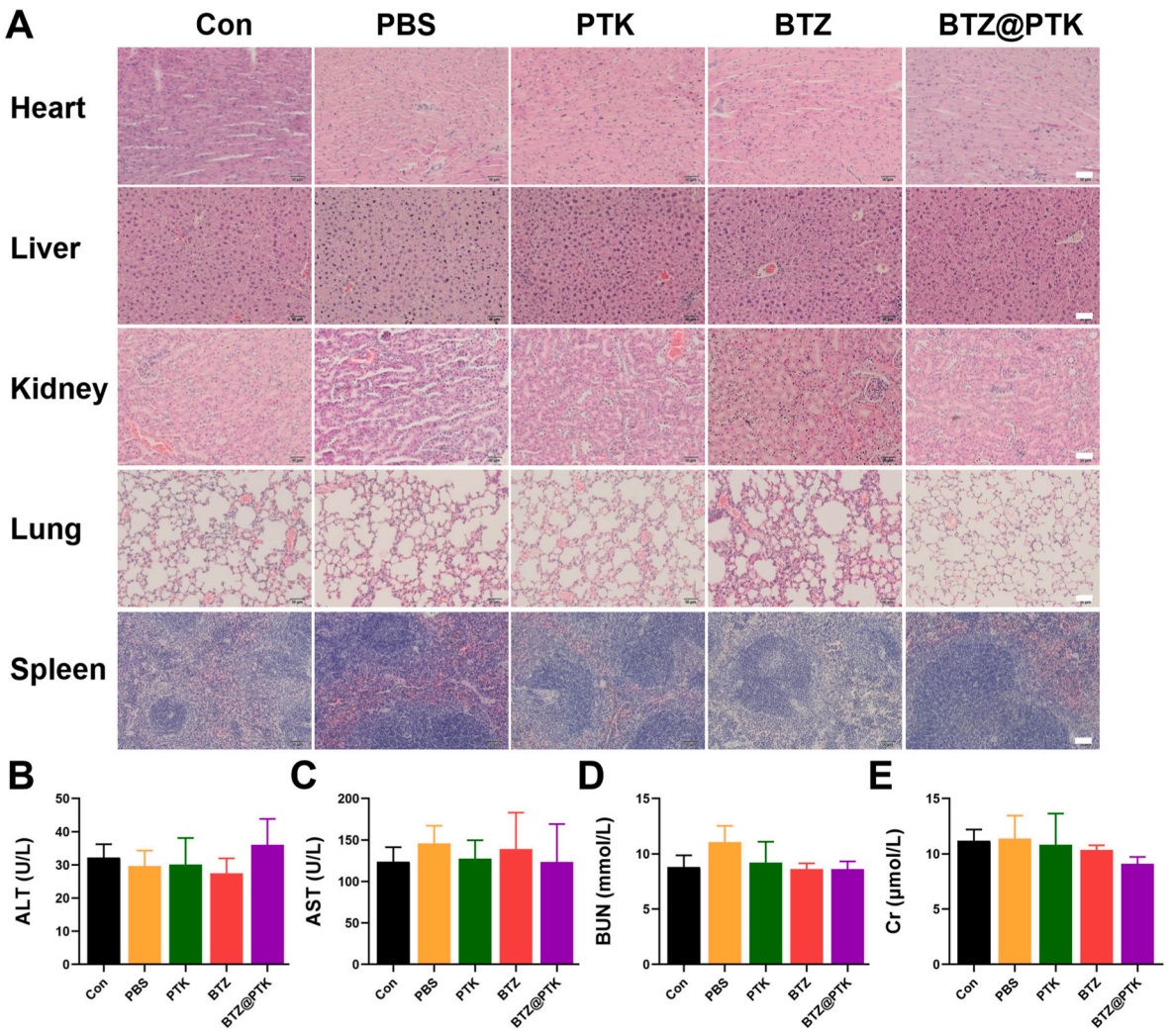

Fig. 10. Effect of BTZ@PTK on chronic toxicity in each group.
(A) Histopathological analysis of heart, liver, spleen, lung, and kidney in each group by H&E staining. Scale bar, 50 μm. Evaluation of the hepatotoxicity and nephrotoxicity of each treatment by measuring the serum levels of ALT (B), AST (C), BUN (D) and Cr (E). Data are represented as mean ± SD, n = 8.

Compared with that of normal mice, macrophages accumulate in OA synovial tissue with enhanced M1-like phenotype whereas the injection of BTZ@PTK could reduce its level to a different extent (Fig. 8A). Furthermore, BTZ@PTK effectively resulted in a drop in the proportion of M1-like macrophages (Fig. 8B). As expected, the BTZ@PTK displayed the most obvious inhibition of M1 macrophage polarization, which contributed to the block inflammatory response.

Studies have shown that M1-polarised macrophages in synovium release high levels of inflammatory cytokines including IL-6, IL-1β, and TNF-α, which promote chondrocyte hypertrophic differentiation [45,46], resulting in the disruption of cartilage homeostasis. Combined with the efficient blocking of inflammation factors by BTZ@PTK *in vivo*, we hypothesized BTZ@PTK promoted the M1 phenotypic, boosting anti-inflammatory capabilities and thereby delaying damaging processes in chondrocytes.

In addition, according to the *in vitro* flow cytometric results that BTZ@PTK promoted apoptosis of LPS-induced M1 inflammatory macrophages, we further used OA model to confirm whether BTZ@PTK promotes synovial macrophages apoptosis by TUNEL staining. The data demonstrated a consistent trend to cell phenotype, there was increased apoptosis in synovium after BTZ@PTK treatment compared to PBS group (Fig. 8C). Furthermore, treatment with BTZ@PTK significantly increased the number of TUNEL-positive cells to 17.07% versus with 5.31% in the PBS-treated OA model group (Fig. 8D). Taken together, these findings demonstrate that BTZ@PTK could inhibit synovitis may through M1 macrophage apoptosis, which is significantly better than that of the commercial drug of BTZ.

3.13. BTZ inhibits JAK/STAT signaling to block LPS-activiated inflammatory response

To further explore the molecular mechanisms underlying BTZ treatment against inflammatory microenvironment of OA, we performed bioinformatics analysis of mRNA transcriptomes towards BTZ-treated stimulated RAW264.7 cells. We analyzed the data and found that there were 850 differentially expressed genes (DEGs) in PBS vs BTZ (adjusted 1.5 fold, p-value <0.05) (Fig. 9A). Then we collected 198 inflammatory-associated genes in the database (Table S2). A comparison of the above two gene clusters identified 21 intersection genes in PBS vs BTZ/inflammatory-related genes database through Venn analysis (Fig. 9B). Subsequently, we checked the differential gene expression of the 21 intersected genes using R-language, in which 16 genes were downregulated and 5 were upregulated (Fig. 9C). Go and KEGG analysis found that there were two identical signaling pathways affected in PBS vs BTZ groups, including the JAK/STAT signaling pathway and the PI3K-Akt signaling pathway (Fig. 9D and **E**).

JAK/STAT signaling have been reported as a pivotal inflammatory signaling pathway [50]. When LPS ligands bind to JAK1 and JAK2

receptors, receptor-associated JAK can be activated, then activated JAK phosphorylate STATs, STATs in turn translocate into nucleus where they can bind to specific promoter regions of target genes such as pro-inflammatory mediators, thereby triggering inflammation [50]. To gain a more comprehensive understanding of the mechanism on that BTZ targets the JAK/STAT signaling pathway, we determined several crucial proteins of JAK/STAT signaling by Western blotting. It can be seen that the phosphorylation levels of both JAK1 and JAK2 were markedly elevated in LPS-stimulated RAW264.7 cells, suggesting an enhanced activity of JAK1 and JAK2 in response to LPS stimulation. However, the upregulation of both phosphorylated-JAK1 (p-JAK1) and phosphorylated-JAK2 (p-JAK2) levels could be well inhibited by BTZ (Fig. 9F–H). Meanwhile, BTZ blocked the activation of p-STAT3 in LPS-stimulated RAW264.7 cells (Fig. 9I and J). Thus, BTZ may suppress the JAK/STAT signaling pathway in LPS-induced M1 macrophages. providing a potential therapeutic approach for alleviating inflammation.

3.14. Safety evaluation

At the endpoint, the *in vivo* toxicity of BTZ@PTK was investigated by measuring the levels of serum aspartate transaminase (AST), alanine transaminase (ALT) and blood urea nitrogen (BUN), creatinine (Cr) in each group and evaluating histological sections of their primary organs. Relative to the healthy control, there was no discernible changes in the H&E-stained heart, liver, spleen, lung, and kidney (Fig. 10A). Furthermore, there were no evident changes in the serum of AST, ALT levels (Fig. 10B and **C**) and BUN, Cr levels (Fig. 10D and **E**) after treatment with BTZ@PTK versus the PBS group, indicating no hepatotoxicity or nephrotoxicity. Consequently, BTZ@PTK present a good biosafety for OA therapy.

4. Conclusion

In summary, we developed BTZ@PTK that can alleviate inflammation by synergistic ROS down-regulation and M1 macrophages reduction for effective OA treatment. With ROS scavenging ability and ROS-modulated drug release behavior, the BTZ@PTK has considerably better efficacy than BTZ with good biosafety. BTZ@PTK alleviated pain and joint dysfunction, reduced synovium swelling, and delayed the development and progression of OA. Mechanistic studies indicated that BTZ@PTK suppressed the inflammation response via promoting M1 macrophage apoptosis and inhibiting M1 macrophage polarization. These results strongly support that BTZ@PTK exerts an anti-catabolic and anti-inflammatory effect as well as has significant potential treatment for OA. This study also provides a novel platform for inflammation disease associated with high oxidative stress.

CRediT authorship contribution statement

Chunchun Xue: Data curation, Formal analysis, Funding acquisition, Investigation, Writing – original draft. **Jia Tian:** Data curation, Methodology, Writing – review & editing. **Zepeng Cui:** Data curation, Formal analysis, Investigation, Visualization. **Yang Liu:** Data curation, Investigation, Methodology. **Dawei Sun:** Data curation, Formal analysis. **Mengting Xiong:** Data curation, Formal analysis. **Nanxing Yi:** Data curation, Formal analysis. **Kaiqiang Wang:** Data curation, Formal analysis. **Xiaofeng Li:** Formal analysis, Funding acquisition. **Yongjun Wang:** Conceptualization, Funding acquisition, Supervision. **Hao Xu:** Conceptualization, Supervision, Writing – review & editing. **Weian Zhang:** Conceptualization, Funding acquisition, Methodology, Supervision, Writing – review & editing. **Qianqian Liang:** Conceptualization, Funding acquisition, Methodology, Supervision, Writing – review & editing.

Declaration of competing interest

The authors declare that they have no known competing financial interests or personal relationships that could have appeared to influence the work reported in this paper.

Acknowledgments

This work was supported by the following grants: National Natural Science Foundation (no.81920108032, 81873321, 81930116, 81973881, 81804122 and 52333014), State Administration of Traditional Chinese Medicine - Young Qhuang Scholar, New interdisciplinary research Project of Shanghai Municipal Health Commission (no.2022JC005), Traditional Chinese Medicine Research Project Innovation Team Project of Shanghai Health Commission (no.2022CX001), Shanghai "Science and Technology Innovation Action Plan" medical innovation research project (no. 21Y11921400), Shanghai Top Priority Research Center Construction Project (no. 2022ZZ01009), Shanghai University of TCM Xinglin Scholars Project (no. TCM[2020]23) and Shanghai University of TCM Excellent Talents Training Program (no. TCM[2020]10).

Appendix A. Supplementary data

Supplementary data to this article can be found online at https://doi.org/10.1016/j.bioactmat.2023.10.032.

References

[1] A.M. Malfait, R.J. Miller, Emerging targets for the management of osteoarthritis pain, Curr. Osteoporos. Rep. 14 (2016) 260–268, https://doi.org/10.1007/s11914-016-0326-z.
[2] David J. Hunter, Sita Bierma-Zeinstra, Osteoarthritis, Lancet 393 (10182) (2019) 1745–1759.
[3] W.H. Robinson, C.M. Lepus, Q. Wang, H. Raghu, R. Mao, T.M. Lindstrom, J. Sokolove, Low-grade inflammation as a key mediator of the pathogenesis of osteoarthritis, Nat. Rev. Rheumatol. 12 (2016) 580–592, https://doi.org/10.1038/nrrheum.2016.136.
[4] J.N. Katz, K.R. Arant, R.F. Loeser, Diagnosis and treatment of hip and knee osteoarthritis: a review, JAMA 325 (2021) 568–578, https://doi.org/10.1001/jama.2020.22171.
[5] A.M. Philp, E.T. Davis, S.W. Jones, Developing anti-inflammatory therapeutics for patients with osteoarthritis, Rheumatology 56 (2017) 869–881, https://doi.org/10.1093/rheumatology/kew278.
[6] M. Kapoor, J. Martel-Pelletier, D. Lajeunesse, J.P. Pelletier, H. Fahmi, Role of proinflammatory cytokines in the pathophysiology of osteoarthritis, Nat. Rev. Rheumatol. 7 (2011) 33–42, https://doi.org/10.1038/nrrheum.2010.196.
[7] L. Sharma, Osteoarthritis of the knee, N. Engl. J. Med. 384 (2021) 51–59, https://doi.org/10.1056/NEJMcp1903768.
[8] H. Zhang, C. Lin, C. Zeng, Z. Wang, H. Wang, J. Lu, X. Liu, Y. Shao, C. Zhao, J. Pan, S. Xu, Y. Zhang, D. Xie, D. Cai, X. Bai, Synovial macrophage M1 polarisation exacerbates experimental osteoarthritis partially through R-spondin-2, Ann. Rheum. Dis. 77 (2018) 1524–1534, https://doi.org/10.1136/annrheumdis-2018-213450.
[9] T.L. Fernandes, A.H. Gomoll, C. Lattermann, A.J. Hernandez, D.F. Bueno, M. T. Amano, Macrophage: a potential target on cartilage regeneration, Front. Immunol. 11 (2020), https://doi.org/10.3389/fimmu.2020.00111.
[10] Z. Chen, H. Zhong, J. Wei, S. Lin, Z. Zong, F. Gong, X. Huang, J. Sun, P. Li, H. Lin, B. Wei, J. Chu, Inhibition of Nrf2/HO-1 signaling leads to increased activation of the NLRP3 inflammasome in osteoarthritis, Arthritis Res. Ther. 21 (2019), https://doi.org/10.1186/s13075-019-2085-6.
[11] N.B. Tudorachi, E.E. Totu, A. Fifere, V. Ardeleanu, V. Mocanu, C. Mircea, I. Isildak, K. Smilkov, E.M. Cărăuşu, The implication of reactive oxygen species and antioxidants in knee osteoarthritis, Antioxidants 10 (2021), https://doi.org/10.3390/antiox10060985.
[12] P. Lepetsos, K.A. Papavassiliou, A.G. Papavassiliou, Redox and NF-κB signaling in osteoarthritis, Free Radic. Biol. Med. 132 (2019) 90–100, https://doi.org/10.1016/j.freeradbiomed.2018.09.025.
[13] J.A. Bolduc, J.A. Collins, R.F. Loeser, Reactive oxygen species, aging and articular cartilage homeostasis, Free Radic. Biol. Med. 132 (2019) 73–82, https://doi.org/10.1016/j.freeradbiomed.2018.08.038.
[14] R. Liu-Bryan, R. Terkeltaub, Emerging regulators of the inflammatory process in osteoarthritis, Nat. Rev. Rheumatol. 11 (2015) 35–44, https://doi.org/10.1038/nrrheum.2014.162.
[15] W. Zhao, H. Wang, Y. Han, H. Wang, Y. Sun, H. Zhang, Dopamine/phosphorylcholine copolymer as an efficient joint lubricant and ROS scavenger for

the treatment of osteoarthritis, ACS Appl. Mater. Interfaces 12 (2020) 51236–51248, https://doi.org/10.1021/acsami.0c14805.
[16] Q. Zhang, S. Lin, S. Shi, T. Zhang, Q. Ma, T. Tian, T. Zhou, X. Cai, Y. Lin, Anti-inflammatory and antioxidative effects of tetrahedral DNA nanostructures via the modulation of macrophage responses, ACS Appl. Mater. Interfaces 10 (2018) 3421–3430, https://doi.org/10.1021/acsami.7b17928.
[17] J. Kim, H.Y. Kim, S.Y. Song, S.H. Go, H.S. Sohn, S. Baik, M. Soh, K. Kim, D. Kim, H. C. Kim, N. Lee, B.S. Kim, T. Hyeon, Synergistic oxygen generation and reactive oxygen species scavenging by manganese ferrite/ceria Co-decorated nanoparticles for rheumatoid arthritis treatment, ACS Nano 13 (2019) 3206–3217, https://doi.org/10.1021/acsnano.8b08785.
[18] W. Wang, X. Lin, H. Xu, W. Sun, E.M. Bouta, M.J. Zuscik, D. Chen, E.M. Schwarz, L. Xing, Attenuated joint tissue damage associated with improved synovial lymphatic function following treatment with bortezomib in a mouse model of experimental posttraumatic osteoarthritis, Arthritis Rheumatol. 71 (2019) 244–257, https://doi.org/10.1002/art.40696.
[19] S.W. Lee, J.H. Kim, Y.B. Park, S.K. Lee, Bortezomib attenuates murine collagen-induced arthritis, Ann. Rheum. Dis. 68 (2009) 1761–1767, https://doi.org/10.1136/ard.2008.097709.
[20] W. Hu, W. Zhang, F. Li, F. Guo, A. Chen, Bortezomib prevents the expression of MMP-13 and the degradation of collagen type 2 in human chondrocytes, Biochem. Biophys. Res. Commun. 452 (2014) 526–530, https://doi.org/10.1016/j.bbrc.2014.08.102.
[21] J. Wang, Y. Fang, R. Andrea Fan, C.J. Kirk, Proteasome inhibitors and their pharmacokinetics, pharmacodynamics, and metabolism, Int. J. Mol. Sci. 22 (2021), https://doi.org/10.3390/ijms222111595.
[22] S.S. Glasson, T.J. Blanchet, E.A. Morris, The surgical destabilization of the medial meniscus (DMM) model of osteoarthritis in the 129/SvEv mouse, Osteoarthritis Cartilage 15 (2007) 1061–1069, https://doi.org/10.1016/j.joca.2007.03.006.
[23] H. Xu, E.M. Bouta, R.W. Wood, E.M. Schwarz, Y. Wang, L. Xing, Utilization of longitudinal ultrasound to quantify joint soft-tissue changes in a mouse model of posttraumatic osteoarthritis, Bone Res 5 (2017), https://doi.org/10.1038/boneres.2017.12.
[24] Y. Liu, J. Jin, H. Xu, C. Wang, Y. Yang, Y. Zhao, H. Han, T. Hou, G. Yang, L. Zhang, Y. Wang, W. Zhang, Q. Liang, Construction of a pH-responsive, ultralow-dose triptolide nanomedicine for safe rheumatoid arthritis therapy, Acta Biomater. 121 (2021) 541–553, https://doi.org/10.1016/j.actbio.2020.11.027.
[25] V. Krenn, L. Morawietz, G.R. Burmester, R.W. Kinne, U. Mueller-Ladner, B. Muller, T. Haupl, Synovitis score: discrimination between chronic low-grade and high-grade synovitis, Histopathology 49 (2006) 358–364, https://doi.org/10.1111/j.1365-2559.2006.02508.x.
[26] S.S. Glasson, M.G. Chambers, W.B. Van Den Berg, C.B. Little, The OARSI histopathology initiative - recommendations for histological assessments of osteoarthritis in the mouse, Osteoarthritis Cartilage 18 (2010), https://doi.org/10.1016/j.joca.2010.05.025.
[27] W. Ying, P.S. Cheruku, F.W. Bazer, S.H. Safe, B. Zhou, Investigation of macrophage polarization using bone marrow derived macrophages, J. Vis. Exp. (2013), https://doi.org/10.3791/50323.
[28] Y.E. Henrotin, P. Bruckner, J.P.L. Pujol, The role of reactive oxygen species in homeostasis and degradation of cartilage, Osteoarthritis Cartilage 11 (2003) 747–755, https://doi.org/10.1016/S1063-4584(03)00150-X.
[29] A. Ostalowska, E. Birkner, M. Wiecha, S. Kasperczyk, A. Kasperczyk, D. Kapolka, A. Zon-Giebel, Lipid peroxidation and antioxidant enzymes in synovial fluid of patients with primary and secondary osteoarthritis of the knee joint, Osteoarthritis Cartilage 14 (2006) 139–145, https://doi.org/10.1016/j.joca.2005.08.009.
[30] S. Wang, W.X. Ren, J.T. Hou, M. Won, J. An, X. Chen, J. Shu, J.S. Kim, Fluorescence imaging of pathophysiological microenvironments, Chem. Soc. Rev. 50 (2021) 8887–8902, https://doi.org/10.1039/d1cs00083g.
[31] A. Mobasheri, M.P. Rayman, O. Gualillo, J. Sellam, P. Van Der Kraan, U. Fearon, The role of metabolism in the pathogenesis of osteoarthritis, Nat. Rev. Rheumatol. 13 (2017) 302–311, https://doi.org/10.1038/nrrheum.2017.50.
[32] S. Nakagawa, Y. Arai, O. Mazda, T. Kishida, K.A. Takahashi, K. Sakao, M. Saito, K. Honjo, J. Imanishi, T. Kubo, N-acetylcysteine prevents nitric oxide-induced chondrocyte apoptosis and cartilage degeneration in an experimental model of osteoarthritis, J. Orthop. Res. 28 (2010) 156–163, https://doi.org/10.1002/jor.20976.
[33] P. Sawle, R. Foresti, B.E. Mann, T.R. Johnson, C.J. Green, R. Motterlini, Carbon monoxide-releasing molecules (CO-RMs) attenuate the inflammatory response elicited by lipopolysaccharide in RAW264.7 murine macrophages, Br. J. Pharmacol. 145 (2005) 800–810, https://doi.org/10.1038/sj.bjp.0706241.
[34] S. Gordon, Alternative activation of macrophages, Nat. Rev. Immunol. 3 (2003) 23–35, https://doi.org/10.1038/nri978.
[35] S. Gordon, F.O. Martinez, Alternative activation of macrophages: mechanism and functions, Immunity 32 (2010) 593–604, https://doi.org/10.1016/j.immuni.2010.05.007.
[36] D. Li, S. Ni, K.S. Miao, C. Zhuang, PI3K/Akt and caspase pathways mediate oxidative stress-induced chondrocyte apoptosis, Cell Stress Chaperones 24 (2019) 195–202, https://doi.org/10.1007/s12192-018-0956-4.
[37] A.E. Dubin, A. Patapoutian, Nociceptors: the sensors of the pain pathway, J. Clin. Invest. 120 (2010) 3760–3772, https://doi.org/10.1172/JCI42843.
[38] S.N. Edd, J. Favre, K. Blazek, P. Omoumi, J.L. Asay, T.P. Andriacchi, Altered gait mechanics and elevated serum pro-inflammatory cytokines in asymptomatic patients with MRI evidence of knee cartilage loss, Osteoarthritis Cartilage 25 (2017) 899–906, https://doi.org/10.1016/j.joca.2016.12.029.
[39] H. Ling, Q. Zeng, Q. Ge, J. Chen, W. Yuan, R. Xu, Z. Shi, H. Xia, S. Hu, H. Jin, P. Wang, P. Tong, Osteoking decelerates cartilage degeneration in DMM-induced osteoarthritic mice model through TGF-β/smad-dependent manner, Front. Pharmacol. 12 (2021), 678810, https://doi.org/10.3389/fphar.2021.678810.
[40] M.D. Smith, E. Barg, H. Weedon, V. Papengelis, T. Smeets, P.P. Tak, M. Kraan, M. Coleman, M.J. Ahern, Microarchitecture and protective mechanisms in synovial tissue from clinically and arthroscopically normal knee joints, Ann. Rheum. Dis. 62 (2003) 303–307, https://doi.org/10.1136/ard.62.4.303.
[41] C. Manferdini, F. Paolella, E. Gabusi, Y. Silvestri, L. Gambari, L. Cattini, G. Filardo, S. Fleury-Cappellesso, G. Lisignoli, From osteoarthritic synovium to synovialderived cells characterization: synovial macrophages are key effector cells, Arthritis Res. Ther. 18 (2016) 83, https://doi.org/10.1186/s13075-016-0983-4.
[42] X. Xu, W. Gao, S. Cheng, D. Yin, F. Li, Y. Wu, D. Sun, S. Zhou, D. Wang, Y. Zhang, R. Jiang, J. Zhang, Anti-inflammatory and immunomodulatory mechanisms of atorvastatin in a murine model of traumatic brain injury, J. Neuroinflammation 14 (2017) 167, https://doi.org/10.1186/s12974-017-0934-2.
[43] W. de Munter, E.J.W. Geven, A.B. Blom, B. Walgreen, M.M.A. Helsen, L.A. B. Joosten, J. Roth, T. Vogl, F.A.J. van de Loo, M.I. Koenders, W.B. van den Berg, P. M. van der Kraan, P.L.E.M. van Lent, Synovial macrophages promote TGF-β signaling and protect against influx of S100A8/S100A9-producing cells after intra-articular injections of oxidized low-density lipoproteins, Osteoarthritis Cartilage 25 (2017) 118–127, https://doi.org/10.1016/j.joca.2016.07.020.
[44] W. Knudson, S. Ishizuka, K. Terabe, E.B. Askew, C.B. Knudson, The pericellular hyaluronan of articular chondrocytes, Matrix Biol. 78–79 (2019) 32–46, https://doi.org/10.1016/j.matbio.2018.02.005.
[45] Z. Fan, B. Bau, H. Yang, S. Soeder, T. Aigner, Freshly isolated osteoarthritic chondrocytes are catabolically more active than normal chondrocytes, but less responsive to catabolic stimulation with interleukin-1β, Arthritis Rheum. 52 (2005) 136–143, https://doi.org/10.1002/art.20725.
[46] Q. Guo, X. Chen, J. Chen, G. Zheng, C. Xie, H. Wu, Z. Miao, Y. Lin, X. Wang, W. Gao, X. Zheng, Z. Pan, Y. Zhou, Y. Wu, X. Zhang, STING promotes senescence, apoptosis, and extracellular matrix degradation in osteoarthritis via the NF-κB signaling pathway, Cell Death Dis. 12 (2021) 13, https://doi.org/10.1038/s41419-020-03341-9.
[47] J. Hu, J. Zhou, J. Wu, Q. Chen, W. Du, F. Fu, H. Yu, S. Yao, H. Jin, P. Tong, D. Chen, C. Wu, H. Ruan, Loganin ameliorates cartilage degeneration and osteoarthritis development in an osteoarthritis mouse model through inhibition of NF-κB activity and pyroptosis in chondrocytes, J. Ethnopharmacol. 247 (2020), 112261, https://doi.org/10.1016/j.jep.2019.112261.
[48] Q. Hu, M. Ecker, Overview of MMP-13 as a promising target for the treatment of osteoarthritis, Int. J. Mol. Sci. 22 (2021) 1742, https://doi.org/10.3390/ijms22041742.
[49] A.M. Bendele, M. Neelagiri, V. Neelagiri, I. Sucholeiki, Development of a selective matrix metalloproteinase 13 (MMP-13) inhibitor for the treatment of Osteoarthritis, Eur. J. Med. Chem. 224 (2021), 113666, https://doi.org/10.1016/j.ejmech.2021.113666.
[50] C.J. Malemud, Negative regulators of JAK/STAT signaling in rheumatoid arthritis and osteoarthritis, Int. J. Mol. Sci. 18 (2017) 484, https://doi.org/10.3390/ijms18030484.